HIGH THROUGHPUT IMAGE ANALYSIS OPTIMIZATION OF BIOLEACHING BACTERIAL BIOFILMS

Arnaud Kolzer

Master Project

Supervised by :

Prof. Mario Vera Véliz - Pontificia Universidad Católica de Chile

Prof. Rizlan Bernier-Latmani – EPFL, Environmental Microbiology Laboratory

December 2020

Acknowledgement

I would like to thank Prof. Mario Vera for giving me the opportunity to carry out my Master Project in his group during this difficult sanitary situation. His plentiful advices and ideas really helped me for the development of my thesis. I also thank Prof. Timothy Rudge for his collaboration and availability for answering to my doubts.

Table of Contents

List of Abbreviations

AHLs : N-acyl-homoserine lactones
AI-2 : Quorum sensing autoinducer- type 2
AMD : Acid Mine Drainage.
BDSF : cis-2-dodecenoic acid
DAPI : 4′,6-diamidino-2-phenylindole.
DEFCoN : Density Estimation by Fully Convolutional Networks
DNA : Deoxyribonucleic Acid.
DSF : cis-11-methyl-dodecenoic acid
DSF_f : Diffusible signal factors
eDNA : Extracellular DNA
EFM : Epifluorescence Microscopy.
EPS : Extracellular Polymeric Substances.
FLOSS : Free/Libre Open Source Software
MAC : Mackintosh medium
MS : Metal sulfides
PQS : *Pseudomonas* quinolone signal
QS : Quorum sensing
RISC : Reduced Inorganic Sulfur Compounds.

Keywords

Acidophilic bacteria; Automatic image analysis; Bacterial biofilm; Bioleaching; Quorum Sensing; Free/Libre Open Source Software

Abstract

Bioleaching is the solubilization of metals sulfides, as pyrite (FeS_2), mediated by a consortium of microorganisms capable to oxidize iron/sulfur. These microorganisms are mainly species of acidophilic bacteria and archaea that are embedded in a biofilm formed of extracellular polymeric substances (EPS). In EPS, intra/interspecies communication can take place, phenomena of great importance to understand bioleaching. One method used to communicate is by quorum sensing (QS), a gene regulation responding to population density, through diffusible signals factors (DSF_f). Studies have already shown that these signals molecules can inhibit the growth of bioleaching bacteria, such as *Leptospirillum ferriphilum*^{T}, but their impact on other acidophilic bioleaching bacteria needs to be determined. Automatic images analysis could lead to improve the comprehension of the mineral colonization in acidophilic bacteria in temporal dynamics and under presence of DSF_f. The aim of this study is to develop an open-source automatic biofilm analysis methodology to quantify colonies population. Open-source software Python and Fiji are used to analyze the effect of DSF_f on *Acidithiobacillus ferriphilus*^{T}*, Acidithiobacillus ferridurans*^{T}, *Acidithiobacillus ferrooxidans*^{T} and *Leptospirillum ferrooxidans*^{T}. We have obtained a new robust automatic methodology that has been validated by analyzing the data used by Bellenberg et al. (2018) and that can conduct to a better understanding of mineral colonization of bioleaching bacteria. We have also discovered that the growth of *A. ferriphilus*^{T} is inhibited under the presence of BDSF and DSF, molecules from the DSF_f family, and that the growth *A. ferridurans*^{T} is inhibited under the presence of BDSF. The methodology created in this project will help to implement machine learning analysis to biofilm images for axenic and mixed cultures.

Résumé

La biolixiviation est la solubilisation de sulfures métalliques, comme la pyrite (FeS_2), par un consortium de micro-organismes capables d'oxyder le fer/soufre. Ces microorganismes sont principalement des espèces de bactéries et d'archées acidophiles qui sont incorporées dans un biofilm formé de substances polymériques extracellulaires (EPS). Dans cet EPS, une communication intra/inter-espèces d'une grande importance pour comprendre la biolixiviation peut avoir lieu. L'une des méthodes utilisées pour communiquer est la détection du quorum (QS), une régulation des gènes en fonction de la densité de population, par le biais de facteurs de signaux diffusibles (DSF_f). Des études ont déjà montré que ces molécules de signaux peuvent inhiber la croissance des bactéries de biolixiviation, tel que *Leptospirillum ferriphilum*^{T}, mais leur impact sur d'autres bactéries doit être déterminé. L'analyse automatique des images pourrait permettre d'améliorer la compréhension de la colonisation minérale chez les bactéries acidophiles dans une dynamique temporelle. L'objectif de cette étude est de développer une méthodologie « open-source » d'analyse automatique de biofilms pour quantifier la population de colonies. Les logiciels libres Python et Fiji sont utilisés pour analyser l'effet de DSF_f sur les bactéries *Acidithiobacillus ferriphilus*^{T}, *Acidithiobacillus ferridurans*^{T}, *Acidithiobacillus ferrooxidans*^{T} et *Leptospirillum ferrooxidans*^{T}. Nous avons obtenu une nouvelle méthode automatique qui est validée par l'analyse des données utilisées par Bellenberg et al. (2018). Nous avons également découvert que la croissance de *A. ferriphilus*^{T} est inhibée en présence de DSF et BDSF, des molécules de la famille des DSF_f, et que la croissance de *A. ferridurans*^{T} est inhibée en présence de BDSF. La méthodologie créée dans ce projet aidera à mettre en place des analyses plus approfondies par « machine learning » des images de biofilms de cultures axéniques et mixtes.

1. Introduction

Bioleaching is described as the solubilization of metals catalyzed by microorganisms, from ores which are often almost insoluble. (Brierley & Brierley, 2013; Martinez et al., 2015; Vera et al., 2013). The microorganisms play the role of enhancer and can be used for different types of metal sulfides (MS), like pyrite (FeS_2) and chalcopyrite ($CuFeS_2$) among others, to recover metals such as copper and nickel. Biological leaching can be found in natural and anthropogenic environments, and it is particularly used in by mining industry in biomining processes. In copper mining, a decrease of high grade ores and an increase of its worldwide demand is observed, with a predicted demand being at least 3 times the actual one in 2100 (Schippers et al., 2018). Thus, it is strongly necessary to be able to collect metals hardly extractable, as in sulfides, in a sustainable way. Biological leaching is responsible for only around 15% of its amount extracted worldwide (Brierley & Brierley, 2013).

MS leaching by microorganisms is facing majors challenges, as mine drainage or acid rock drainage (AMD/ARD) can occur (Henderson, 2018; Vera et al., 2013). AMD is described as the generation of acid effluent which can then enhance the solubilization and transport of toxics metals to fresh water sources. It can be caused in abandoned or active mining sites or in natural environments, and occurs usually in sulfide-aggregated rocks, such as pyrite and chalcopyrite. This pollution can have a strong impact in the environment, contaminating the soils, the surface and even groundwater sources (Henderson, 2018). AMD is an important issue for Chile, due to its typical mineralogy and the high quantity of running and abandoned mining site in the north of the country (Obreque-Contreras et al., 2015). Furthermore, Chile is a country which is strongly dependent on the mining industry, as it extracts the biggest amount of copper worldwide, with 5,787 thousand metric tons in 2019 (Comisión

Chilena del cobre, 2020) (Table 1). It is therefore important for the development of the country to understand the function of bioleaching and the interactions of microorganisms with sulfidic ores, to move towards more sustainable and profitable methods for copper extraction.

Table 1 : Amount of copper produced per country in 2018 and 2019 in metric tons (Comisión Chilena del Cobre, 2020)

PRINCIPALES PRODUCTORES DE COBRE Miles de TM	2018	2019	Var. %
Chile	5.832	5.787	-0,8
Perú	2.437	2.455	0,7
China	1.507	1.601	6,3
Estados Unidos	1.216	3.144	158,5
Resto del Mundo	9.339	7.715	-17,4
Total Mundo	**20.330**	**20.702**	**1,8**

1.1. Bioleaching mechanisms

Bioleaching of MS is conducted by two main processes : direct and indirect leaching (Sand et al., 2001; Schippers, 2004; Vera et al., 2013) (Figure 1). Indirect bioleaching is subdivided in two types, “contact” and “non-contact”. Indirect non-contacts leaching refers to the biological oxidation of iron(II)-ions to iron(III)-ions in the solution, without attachment of the cells to the mineral. Iron(III)-ions oxidize then the mineral to disrupt the sulfide crystals bonds and release the sulfur compounds in the solution.

The indirect contact leaching is using the same processes described above, namely oxidation of iron(II)-ions to iron(III)-ions. This process occurs within a biofilm on the mineral i.e., colonies of microorganisms embedded within a self-produced matrix of extracellular polymeric substances (EPS) (Bellenberg et al., 2014). EPS allows to increase the iron(III)-ions concentration at microbe-mineral interface and therefore enhance its degradation (Sand et al., 2001).

In the direct mechanism, as its name indicates it, the cells would directly oxidize the mineral. The membrane of the bacteria interacts directly with the sulfide through enzymatic mechanisms (Sand et al., 2001). But it is important to note that this process has not been proved until now.

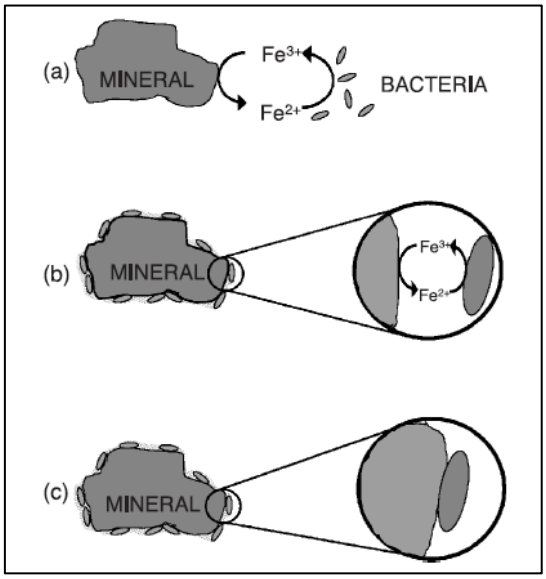

Figure 1 : The different mechanisms of leaching: (a) the indirect mechanism, (b) the indirect contact mechanism, (c) the direct mechanism (Crundwell, 2003)

Bioleaching of metal sulfides has been well studied and different pathways are proposed to explain the degradation of the sulfur moiety: the thiosulfate pathway and the polysulfide pathway (Schippers & Sand, 1999). The thiosulfate pathway explains the oxidation of pyrite, molybdenite (MoS_2) and tungstenite (WS_2). The following equations summarizes the thiosulfate pathway (Schippers & Sand, 1999): After the disruption of the bond between the iron and the metal, the sulfur moiety is oxidized to a soluble compound, thiosulfate (Equation 1). This compound is further oxidized to different sulfur compound, as tetrathionate, trithionate, pentathionate, and elemental sulfur (S^0), to finally produce sulfate (Equation 2).

(1) $$FeS_2 + 6\,Fe^{3+} + 3H_2O \rightarrow\ {S_2O_3}^{2-} + 6\,Fe^{2+} + 6\ H^+$$

(2) $${S_2O_3}^{2-} +\ 8\,Fe^{3+} +\ 5H_2O \rightarrow\ {SO_4}^{2-} + 8\,Fe^{2+} + 10\ H^+$$

The polysulfide pathway is used to explain the dissolution of metal sulfides such as orpiment (As_2S_3) chalcopyrite ($CuFeS_2$), galena (PbS) or sphalerite (ZnS). The oxidation of the sulfur moiety result on the formation of S° through a series of reaction via polysulfides (Equation 3 and 4). This can then be oxidized biologically to produce sulfuric acid (Equation 5) as shown in the following polysulfide pathway equations (Schippers & Sand, 1999):

(3) $$MS +\ Fe^{3+} + H^+ \rightarrow\ M^{2+} + 0.5\,H_2S_n + Fe^{2+}\ (n \geq 2)$$

(4) $$0.5\,H_2S_n +\ Fe^{3+} \rightarrow 0.125\,S_8 + Fe^{2+} +\ H^+$$

(5) $$0.125\,S_8 + 1.5O_2 + H_2O \rightarrow {SO_4}^{2-} + 2H^+$$

In both, thiosulfate and polysulfide pathway, the regeneration of iron(III)-ions is driven by the leaching bacteria, which is their main role in bioleaching (Figure 2).

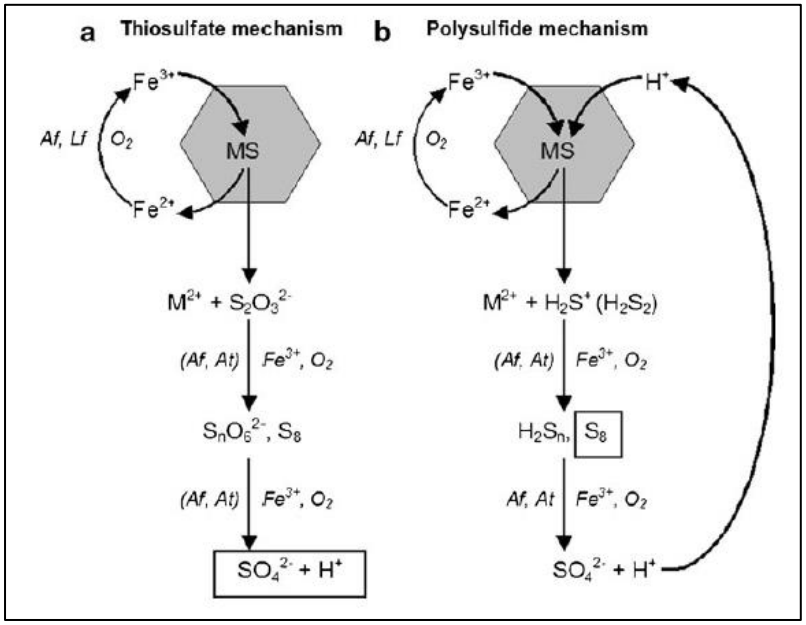

Figure 2 : Pathways of metal sulfide oxidation: (a) thiosulfate pathway and (b) polysulfide pathway (Schippers & Sand, 1999, modified).

1.2. Leaching microorganisms

1.2.1. Generalities

Dissolution of MS is mainly conducted in acidic environment with a pH below 3, by microorganisms that can oxidize iron(II)-ions and/or reduced inorganic sulfur compounds (RISC). These acidophilic microorganisms were mostly discovered in acid mine drainage. Despite the limited type of substrate, the high acidity and the high levels of metal ions and sulfate, these mining biotopes tend to have a great microbial diversity. This diversity consists of oxidizers which can grow heterotrophically, autotrophically or mixotrophically at several temperatures, ranging from near 0°C to 100 °C. They are therefore described either as psychrophilic, mesophilic, moderately thermophilic or extremely thermophilic (Diao et al., 2014; Rohwerder et al., 2003; Vera et al., 2013). Generally, the microorganisms living at high temperature, the extremely thermophilic, belong to the archaeal domain, while the ones living at low temperature, psychrophiles, consist of bacteria. The mesophilic and moderately thermophilic can be

either bacteria or archaea (Rohwerder et al., 2003). Some common acidophilic microorganisms, their optimum pH and temperature are detailed on the following table.

Table 2 : Summary of common acidophilic microorganisms (Diao et al., 2014)

Acidophilic species	Optimum pH	Optimum temperature (°C)
Iron-oxidizers		
Leptospirillum ferrooxidans	1.5–3.0	28–40
L. ferriphilum	1.3–1.8	45–50
"*Ferrimicrobium acidiphilum*"	2.0–2.5	37
Ferroplasma acidiphilum	1.7	35
Sulfur-oxidizers		
Acidithiobacillus thiooxidans	2.0–3.0	28–30
A. caldus	2.0–2.5	45
Thiomonas cuprina	3.5–4.0	30–36
Metallosphaera spp.	2.0–3.0	70–75
Sulfolobus spp.	2.0–2.6	60–75
Iron- and sulfur-oxidizers		
Acidithiobacillus ferrooxidans	2.5	30–35
Acidianus spp.	1.5–2.0	70–90
Sulfolobus metallicus	2.0–3.0	75
Iron-reducers		
Acidiphilium spp.	2.5–3.5	27–37
Iron-oxidizers/reducers		
Acidimicrobium ferrooxidans	~2	45–50
Iron-oxidizers/reducers and sulfur-oxidizers		
Sulfobacillus spp.	1.6–2.5	37–55

The metabolic capacity of leaching microorganisms is also made up of a wide range of possibilities. Indeed, it can be limited to a specific substrate, for example *Leptospirillum ferrooxidans* and *Leptospirillum ferriphilum* can only live in an aerobic environment by oxidizing aerobically iron(II)-ions. On the other hand, *Acidithiobacillus ferrooxidans* possess a broad metabolic capacity. This species can live aerobically on the oxidation of RISC such as S^0, thiosulfate, tetrathionate and trithionate, or of iron(II)-ions, but it is also capable to oxidize other metal ions, formic acid and molecular hydrogen. Its anaerobic growth is conducted by the iron(III)-ions reduction and the oxidation RISC or hydrogen. Microorganisms can therefore enhance leaching under aerobic or anaerobic conditions, an important detail for AMD. Indeed, common AMD

countermeasures are flooding or organic covering of the tailings or waste heaps, where bioleaching occurs. Thus, these measures would not be efficient and anaerobic bioleaching could remain operating.

Bioleaching in general is performed by mixed communities of microorganisms. The interactions between the species are not totally understood yet. For example, it has been proved that cell attachment and biofilm formation, which are critical factors for bioleaching, of sulfur oxidizing bacteria is improved when primary colonizers, namely iron oxidizing bacteria, are present. (Bellenberg et al., 2014; Buetti-Dinh et al., 2020).

1.2.2. Microorganisms used

1.2.2.1. *Acidithiobacillus ferriphilus* DSM 100412^T

A. ferriphilus^T can live from the oxidation of iron(II)-ions as well as RISC. This species is Gram-negative and strictly chemolithotroph. It grows anaerobically by reducing iron(III)-ions, coupled to the oxidation of RISC or aerobically by oxidizing Iron(II) or RISC, coupled to molecular oxygen. *A. ferriphilus*^{T} is mesophilic, with growth temperatures between 10°C to 33°C, and acidophilic, with a pH optimum of 2 (Falagán & Johnson, 2016).

1.2.2.2. *Acidithiobacillus ferridurans* DSM 29468^T

A. ferridurans^T grows in a temperature between 10°C to 37°C with an optimum at 29°C and a pH range of 1.4 to 3 with an optimum at 2.1. It can grow aerobically or anaerobically, by either coupling the oxidation of iron(II)-ions, RISC or hydrogen to the reduction of oxygen or either by oxidizing hydrogen or reduced sulfur couple to the reduction of iron(III)-ions. *A. ferridurans*^{T} is a Gram-negative bacterium and obligate chemolithoautotrophic (Hedrich & Johnson, 2013).

1.2.2.3. *Acidithiobacillus ferrooxidans* DSM 14882^T

A. ferroxidans^T is a facultative anaerobic, Gram-negative, extreme acidophile and obligate chemolithotroph species. It uses iron(III)-ions, sulfur or oxygen as electron acceptor and hydrogen, RISC and iron(II)-ions as electron donor. *A. ferrooxidans*^{T} has optimal ranges of temperature of 20°C - 35°C and of pH of 1.8 - 2 (Quatrini & Johnson, 2019; Rawlings, 2002)

1.2.2.4. *Leptospirillum ferrooxidans* DSM 2705^T

L. ferrooxidans^T is Gram-negative, chemolithoautotrophic, mesophilic and highly acid tolerant (optimal range pH of 1.5-1.8). It is strictly anaerobic and obtains the energy to grow by oxidizing iron(II)-ions and by reducing oxygen. Unlike the other species, it cannot reduce RISC and its ability of oxidizing iron(II)-ions is not inhibited by iron(III)-ions, due to its high affinity for iron(II)-ions (Rawlings, 2002; Tzvetkova et al., 2002).

1.3. Biofilms

Bioleaching microorganisms usually form biofilms on the surface of MS. In this lifestyle, bacterial cells are embedded in a matrix of EPS self-produced and represent less than 10% of the dry mass of the biofilm (Flemming & Wingender, 2010). The 90% is accounted by EPS matrix that consists of proteins, lipids, extracellular DNA (e-DNA) and polysaccharides (Bellenberg et al., 2014; Flemming et al., 2007). EPS are important for the cells because it allows them to have a good adhesion to the mineral, to be immobilized, to stay in proximity and to improve the cohesion of the biofilm. These characteristics provide better interactions and communication between biofilm members. Others functions of EPS matrix are retention of water to keep a hydrated environment around the microorganisms, the interaction with the environment, to

protect cells in case of environment variations and to act as nutrient source, among others (Flemming et al., 2007; Flemming & Wingender, 2010; Garnett & Matthews, 2012).

The attachment and formation of biofilm can be influenced by environmental factors, for example the nature of the surface, the availability of nutrients, the temperature, the presence of oxygen, pH and also by the microorganisms embedded in the EPS matrix (Bosecker, 1997; Flemming et al., 2007). The biofilm development is divided in multiples stages; the first one is the initial attachment of a single planktonic cell on the substrate. This step is highly reversible, and the bacteria often needs to create adhesion molecules for a better attachment. The second stage is the division of the cells and the formation of microcolonies, that leads to interspecies interactions. The EPS matrix is then secreted allowing to develop a three-dimensional architecture. With the time, these colonies grow to form a mature biofilm, composed of a heterogenous disposition of cells and molecules. Finally, depending on environmental signals, the biofilm releases planktonic cells that disperse and colonize new environments (Figure 3) (Flemming & Wingender, 2010; Garnett & Matthews, 2012).

Bioleaching bacteria create very special biofilms that are mainly composed of layers in laboratory conditions. Studies also indicated that its attachment does not occur randomly on the metals sulfides as the bioleaching microorganisms prefer attach to sites with surface imperfections (Vera et al., 2013). The mechanisms of biofilm lifestyle on MS are not totally understood yet. A better understanding on their formation and attachment could lead to improvement on bioleaching comprehension and implementation on large scale (Zhang et al., 2019).

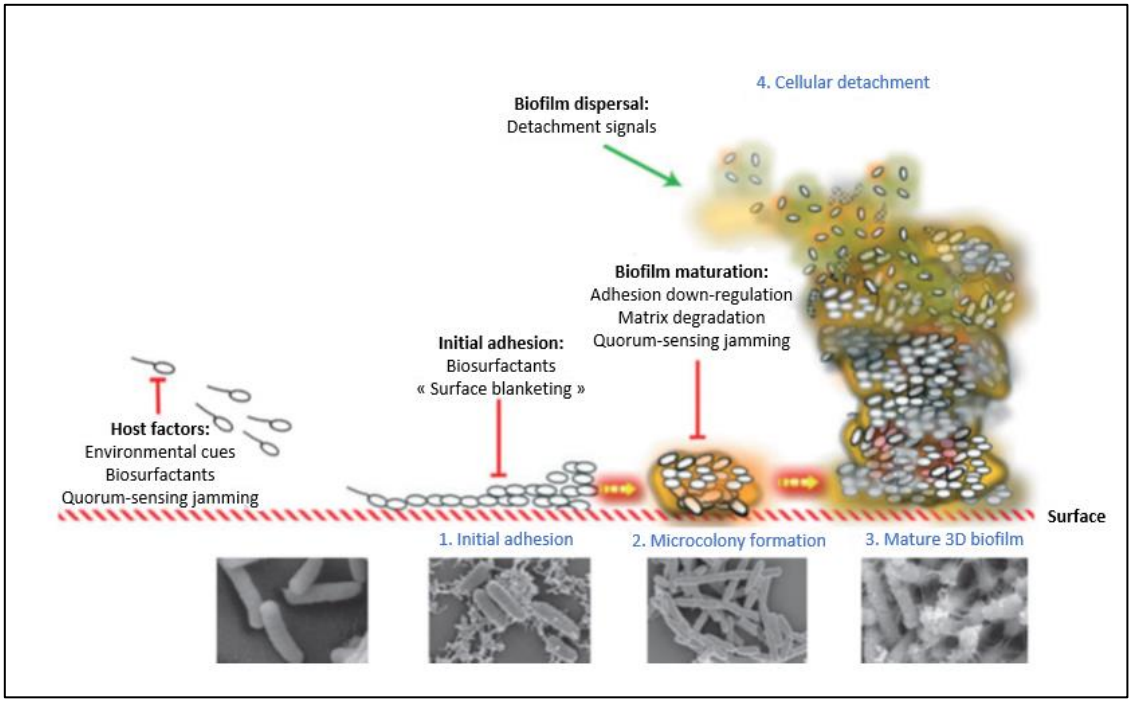

Figure 3 : Stages of biofilm formation (Rendueles & Ghigo, 2012)

During the maturation of the biofilm, the cells release diverse molecules in the matrix, not only to build the biofilm and protect the bacteria, but also to send signals to other cells. This communication aims to a better functioning and regulated biofilm and that can be done by quorum sensing (QS) (Rendueles & Ghigo, 2012).

1.4. Quorum sensing

1.4.1. Generalities

QS is described as the gene regulation, depending on the population density of the community. This density and dose-dependent system is activated when a certain number of cells, or quorum, is exceeded. The quorum is sensed through signaling molecules, or autoinducers, that accumulate in the environment. Once their concentration reaches a threshold, they activate changes in gene expression by binding with protein receptors. Quorum sensing can control many bacterial phenotypes, such as their competence, virulence factor secretion, sporulation,

bioluminescence and biofilm formation (Bassler & Losick, 2006; Monnet & Gardan, 2015). QS is important for the cooperation between bacteria, but it can also be used when competition is involved, by the existence of QS quenching systems (Cheng et al., 2010; Rendueles & Ghigo, 2012). This type of communication allows the cell-to-cell communication and therefore social activity, or “social microbiology”, to be established (Della Sala et al., 2019; Rendueles & Ghigo, 2012). QS is present in Gram positive and Gram negative bacteria, but they use different molecules to communicate (Bassler & Losick, 2006).

1.4.2. QS in Gram-positive bacteria

The system used predominantly by Gram-positive quorum sensing bacteria is a type of bi-component sensing oligopeptides (Bassler & Losick, 2006; J. Zhou & Cai, 2018). These autoinducing peptides (AIPs) are created in the ribosome, modified inside the cell and transported to the extracellular environment. Once their threshold concentration is reached, the peptide can, by activating a histidine kinase or by reinternalization, alter the expression of the target genes (Kim & Yeon, 2018; Monnet & Gardan, 2015).

1.4.3. QS in Gram-negative bacteria

Gram-negative bacteria produce different classes of autoinducers. The main ones are the following; the N-acyl-homoserine lactones (AHLs), or autoinducer-1, the autoinducer-2 (AI-2), the *Pseudomonas* quinolone signal (PQS) and the family of diffusible signal factors (DSF_f) (Della Sala et al., 2019).

AHLs are synthetized by LuxI-type AHL synthases and consist of a homoserine lactone ring bound to a fatty acyl chain that can have a different saturation degree, oxidation state at β-position, and length. When the quorum of AHLs is attained in the

cell environment, due to a high cell density, the acyl-homoserine lactones activate the LuxR receptor protein in the intracellular space, by entering again the cells through special transporter channels. LuxR is working as a transcription factor for different genes of the cells (Aguilar et al., 2009; Banerjee & Ray, 2016; Della Sala et al., 2019; Kim & Yeon, 2018). Studies have demonstrated that bioleaching bacteria such as *A. ferrooxidans*, *A. ferrivorans* and *Acidiferrobacter sp*. strain SPIII/3 produce AHLs, and that these systems are involved especially in the adhesion and biofilm formation to MS and S° (Bellenberg et al., 2014; González et al., 2013; Ruiz et al., 2008).

The family of AI-2 molecules is made of different cyclic furanone compounds that enter the cell once they rich a limit concentration. Insight the bacterium, they interact with the LuxP/LuxQ receptor kinase complex situated in the membrane, inducing through a chain reaction the inhibition of the expression of regulatory RNAs, turning on expression of virulence determinants (Della Sala et al., 2019)

The third class of signals, the PQSs, include the derivatives of 4-hydroxy-2-heptylquinoline and its dehydroxylated derivatives, as the 2-heptyl-3,4-dihydroxyquinoline, or PQS. These autoinducers are used by different species of *Burkholderia* and *Pseudomonas* and turn on the biofilm formation, the synthesis of toxins and further QS molecules by activating virulence factors regulators (Della Sala et al., 2019).

The DSF_f of autoinducers is made up of cis-2-unsaturatd fatty acids containing different branching and chain length. It is divided in three different categories depending on the genomic context of the QS systems. The first one is represented by *Xanthomonas campestris*, in which the DSF_f is produced by a DSF synthase, the RpfF. With its increase in concentration, the DSF_f binds to the RpfC kinase sensor. This

binding activates a phosphorelay-cascade and the RpfG response regulator. The degradation of cyclic di-GMP is then enhanced and inhibits the global transcription factor Clp. This reaction activates the expression of different genes encoding virulence factor production or biofilm formation (Della Sala et al., 2019). The second category uses a similar system, with the only difference being the regulation of cyclic di-GMP by the RpfR sensor. The last category uses an enoyl-coenzyme A hydratase Dspl to biosynthesize the DSF_f. The mechanisms of perception of the autoinducers have not been fully discovered yet (Della Sala et al., 2019; L. Zhou et al., 2017). The main molecules of the DSF_f autoinducers are family the cis-11-methyl-dodecenoic acid, known as DSF, and the cis-2-dodecenoic acid, known as BDSF (Figure 4) (Della Sala et al., 2019).

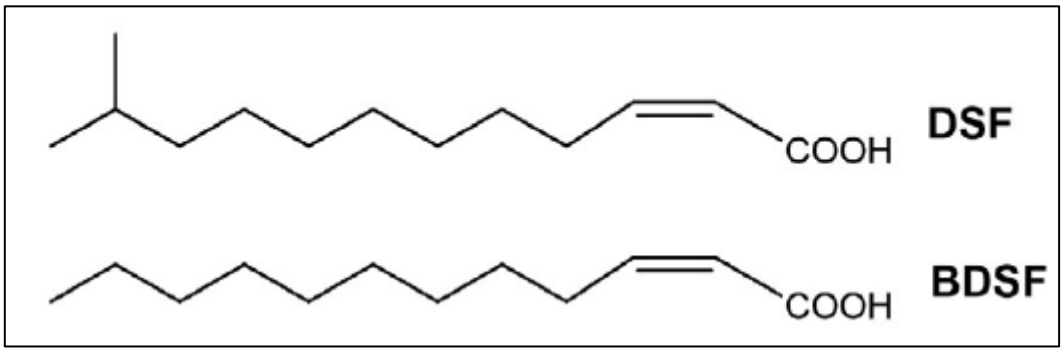

Figure 4 : Structure of DSF and BDSF molecules (Della Sala et al., 2019)

It has been shown that some leaching bacteria contain homologous genes of the first category of DSF_f systems. Indeed, Christel et al. (2018) described *rpfF*, *rpfG* and *rpfC* homologous genes, as well as three LuxR family transcriptional regulators protein-encoding genes in the *L. ferriphilum*^{T} genome. It has also been shown that in axenic cultures of *L. ferriphilum*^{T} and *Sulfobacillus thermosulfidooxidans*^{T}, DSF_f inhibit chalcopyrite dissolution and iron(II)-ions oxidation and enhance the dispersion of the biofilm. The growth inhibition has also been observed in mixed culture of the

aforementioned two species together, with addition of *Acidithiobacillus caldus* (Bellenberg et al., 2014). This indicates that bioleaching and bacterial dispersion in multispecies biofilms could be regulated through several QS systems in acidophiles.

1.5. Image Analysis

One of the best tools for biofilm analysis is epifluorescence microscopy (EFM). In general, image analysis is assessed trough private EFM software that have restricted access. Knowledge sharing and spreading can be limited by these aspects, as all the laboratories or research groups do not have the same software tools. The use of Free/Libre Open-Source Software (FLOSS) can be applied to tackle these limitations. FLOSS, Python's scripts are often used as they allow a complete personalization of the coding and of the analysis of the images. Fluorescence's images of bacteria and bioleaching colonies have already been analyzed through Python in different investigations (Bellenberg et al., 2018; Buetti-Dinh et al., 2020), which give tools and knowledge for further investigation, but the scripts were unfortunately not made publicly available. Python is limited by the need of knowing coding and its language, this limitation can be overcome by using Fiji ("Fiji is just ImageJ") (Schindelin et al., 2012, 2015; Schneider et al., 2012), an open-source platform for the treatment and the analysis of images through the use of plugin and macros. Fiji is a well-known FLOSS that contains several different user-written plugins, that are constantly under improvement. Fiji and Python are software that give the possibilities of analyzing high quantity of images automatically, a very important aspect for biofilm studies. This allows to move from single/few image analysis to robust pipelines for semi/quantitative image analysis, for to improving the comprehension of spatial and temporal dynamics of mineral colonization in acidophilic bacteria (Bellenberg et al., 2018). The implementation of such semi/quantitative analysis could lead to more advanced

computational methods, such as machine learning, using neural networks to analyze images patterns. Deep learning has recently been used in biofilm analysis of bioleaching bacteria, and it has already showed a real potential, compared to human expert analysis (Buetti-Dinh et al., 2019).

2. Hypothesis and objectives

2.1. Hypothesis

Robust open-source automatic image analysis pipelines will contribute to a better understanding of the effect of QS on biofilms of acidophilic bacteria.

2.2. Objectives

2.2.1. Main objective

To quantify biofilm formation dynamics of different bioleaching microorganisms through open access automatic image analysis.

2.2.2. Secondary objectives

1- To optimize a methodology to analyze a high number of biofilm images through Fiji

2- To optimize a Python's script for an automatic quantification of biofilm images

3- To validate the analysis with a re-quantification of available data in Bellenberg et al. (2018), with this new quantification methodology

4- To quantify biofilm growth on pyrite surfaces of *A. ferriphilus*^{T}, *A. ferridurans*^{T}, *A. ferrooxidans*^{T} and *L. ferrooxidans*^{T} under the presence of DSF and BDSF

3. Materials and methodology

3.1. Materials

3.1.1. Strains and media

The strains *A. ferriphilus*^{T}, *A. ferridurans*^{T} , *A. ferrooxidans*^{T} and *L. ferrooxidans*^{T} were cultivated in a 150 mL Mackintosh (MAC) medium at pH 2 with 2% pyrite pulp density as energy source.

3.1.2. Experiment

Axenic cultures of the four species in 3.1.1 were inoculated with a concentration of 10^7 cells/ml on pyrite grains (100 -200 µm). These were incubated at 2% pyrite pulp density at 28°C (Figure 5). Samples were taken and cells were stained with 4′,6-diamidino-2-phenylindole (DAPI), as described (Bellenberg et al., 2018). The mineral grains were imaged 7, 16 and 42 days after the inoculation and on the fifth day, DSF and BDSF were added separately at 5 µM, creating 3 cultures for each species: control, with addition of DSF and with addition of BDSF. Epifluorescence images were taken using the wavelet options, calculating an extended focus image with images of at least 50 z-stacked images (1 µm distance). Background images were taken without fluorescence, but instead with background illumination (behind the specimen), in order to clearly discriminate mineral particle areas from inter-grain regions. For the day 7, 16 and 42, 36 images were taken for each species and each condition; background images and the fluorescent ones. With 4 species, 3 conditions, 3 time points and 2 set of images, a total of 2592 images were taken. These images were kindly provided by Dr. Sören Bellenberg (Linnaeus University, Sweden).

Figure 5 : Workflow detailing the cultivation and EFM imaging of the experiment

3.1.3. Images of dataset used in Bellenberg et al. (2018)

With the collaboration of Dr. Sören Bellenberg (Linnaeus University, Sweden), the images analyzed in the paper “Automated Microscopic Analysis of Metal Sulfide Colonization by Acidophilic Microorganisms” (Bellenberg et al., 2018) were available to compare and validate our methodology for automatization of image analysis.

3.2. Methodology

Image analysis was made using the software Zeiss Zen 2.0 Pro, the software Fiji, and a Python’s script, written in collaboration with Prof. Timothy Rudge from the Institute of Biological and Medical Engineering UC. The treatment of the background images and the images containing cell colonies were conducted differently, as the analysis was different too; the images containing the bacteria were used to calculate the number of colonies, while images of the background were used to calculate the area of the grains.

3.2.1. Colony counting

EFM Images obtained with the software Zeiss Zen 2.0 were firstly exported as JPEG format. Due to the heterogeneous quality of the images, the second step was to

find a software able to treat and denoise the images properly, without losing colonies in the treatment. Different plugins from the software Fiji were tried, such as Non Local Means Denoise (Buades et al., 2011; Darbon et al., 2008), PureDenoise (Luisier et al., 2010) and DeepImageJ (Gómez-de-Mariscal et al., 2019), among others. After testing many software plugins, DeepImageJ was selected to treat the images, a plugin working with pre-trained deep learning models (see Results and Discussion). This plugin has a user-friendly interface, with the objective to spread deep learning models and their use in sciences, without the need of being an expert in coding. The deep learning model used is called “Density Estimation by Fully Convolutional Networks (DEFCoN) - A fluorescent spot counter for single molecule localization microscopy”. The script was written by an EPFL student as a Master Project, in the laboratory of Experimental Biophysics, and highlights the fluorescent colonies present on the images while denoising them. This pre-trained model was trained with an image from *A. ferridurans*^{T}, to make it effective with the new set of images and therefore creating a new model that can be run on all the data. After the creation of the model, the images were treated by the plugin through a batch process in Fiji, with the following macros: run("DeepImageJ Run", "model=defcon_density_map_estimation_arnaud preprocessing=[no preprocessing] postprocessing=[no postprocessing] patch=1588 overlap=100 logging=normal"). After this step, it was possible to count the colonies of the images, through the Python’s script (Annex 1) and through Fiji.

The script allowed first to define parameters as the size of the colonies and the intensity’s threshold. The size of the colonies was set to be with a radius between 0,25 μm to 1,5 μm and the intensity’s threshold to 0,1. Then, the images were loaded, the colonies were detected, and their position and size recorded, using the Panda’s library and a blob detection algorithm, blob_log. This algorithm recognizes bright regions on

black background using the algorithms of the Laplacian of Gaussian, by successively increasing standard deviation and loading them up in a cube, where blobs are local maxima. The parameters were set as following: min_sigma=min_colony_radius/np.sqrt(2), max_sigma=max_colony_radius/np.sqrt(2), num_sigma=10, threshold=threshold, overlap=0.2. To ensure the good functioning of the analysis, it is possible to check one of the files and the colonies' position at the end of the script. Finally, the results were saved in a .csv file.

With Fiji, the first step was to threshold the images. As the treatment through the DEFCoN model was also highlighting the colonies, the threshold was easily feasible and an automatic method was chosen, the Otsu's threshold. After the thresholding, the colonies were counted with the plugin "Analyze particles" and the size and the circularity of the colonies were set as following; the radius of the colonies was chosen to be between 1,54 and 9,25 pixels, which according to the pixel size of EFM images, corresponds to 0,25 μm and 1,5 μm, and the circularity to be between 0 to 1. The results were saved in a .csv file.

The images were also analyzed directly with the Python's script without prior denoising, to evaluate the possibility of gaining time without using Fiji. Most parameters remain unchanged from the analysis with denoising, only the threshold was lowered to 0,012, as there was no highlighting of the colonies and therefore the brightness intensity of the colonies was much lower in comparison with denoised images. The summary of the process to count the colonies is shown in Figure 6.

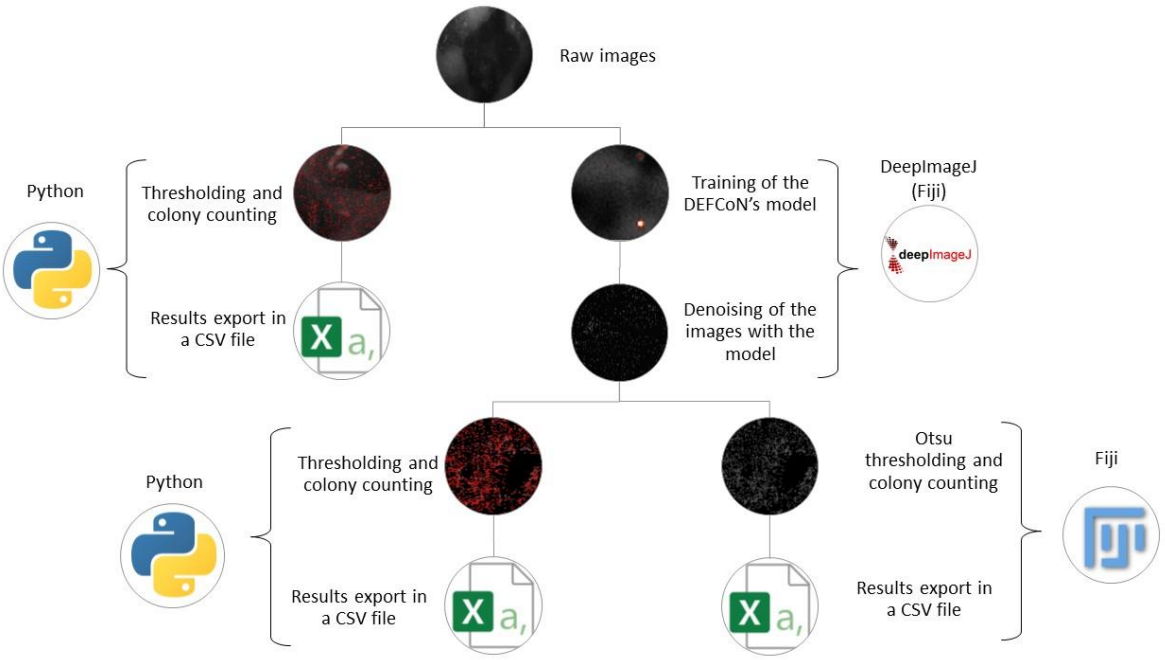

Figure 6 : Summary of the methodology for colony counting

To compare the counting with and without denoising of the images, an analysis of the X, Y positions of the colonies obtained with the Python's script was conducted. A MATLAB's script (Annex 3) compared the location of each colony within a Euclidian distance of 3 pixels and gives the number of colonies having the same coordinate for each image. Such analysis is not feasible with Fiji's results, as the exported files do not contain the X, Y positions of the colonies.

3.2.2. Background Analysis

The corresponding background images of the colonies were analyzed to normalize the colony counting with the area of the grain disponible for their growth. The images were taken with the software Zeiss Zen 2.0 and exported as JPEG files. Unfortunately, once again the images had a poor quality and several of them were out of focus or with a high amount of noise. Therefore, a straight counting of the area with a simple threshold was not realistic and feasible. To differentiate the background from the grain, the choice was made to use a segmentation plugin from Fiji, "Trainable Weka

segmentation” (Arganda-Carreras et al., 2017). It combines a group of selected images’ features to produce pixel-based segmentation through machine learning algorithms provided from the toolkit Waikato Environment for Knowledge Analysis (WEKA). This plugin allows an automated image analysis with a graphical user interface that is easy to access and to understand and works as a bridge between the image processing and the machine learning field. Trainable Weka Segmentation uses by default binary pixel classification and the class must be selected and traced by drawing the region of interest (ROI), thanks to the set of drawing tools present on Fiji, such as rectangle, oval, round rectangular, elliptical and freehand selections, between others. The classifier (or model) and the data can be trained and loaded through this interface. Before the training of the images, it was important to select the features used for the segmentation, in the segmentation settings, as many different methods are available (Figure 7).

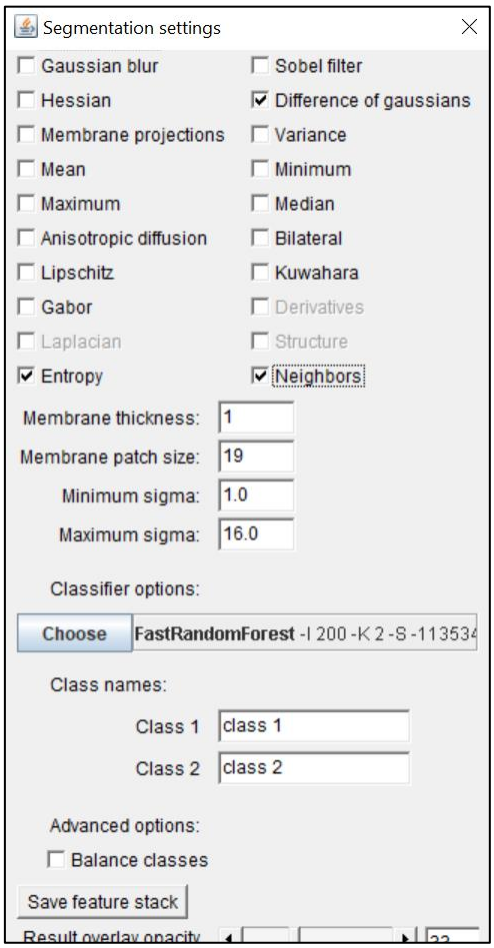

Figure 7: Segmentation settings with the features available for the training of the classifier

The features selected to train the models were the Difference of gaussian, that allows to increase the visibility of edges and therefore the difference between the background and the grain; the Entropy, that allows to reduce the noise of the images and to improve the recognition on the classes; and the Neighbors, to compare each pixels with their neighbors as they have a bigger probability to be identic. The plugin uses the features with the following method, according to Arganda-Carreras et al. (2017):

“Difference of gaussian : calculates two Gaussian blur images from the original image and subtracts one from the other σ values are varied as usual, so $\frac{n(n-1)}{2}$ feature images are added to the stack.

Entropy : draws a circle of radius r around each pixel; gets the histogram of that circle split in numBins chunks; then calculates the entropy as

$\sum_{p\ in\ histogram} -p * log_2(p)$, where p is the probability of each chunk in the histogram. numBins are equal to 32, 64, 128, 256 . r is equal to σ.

Neighbors : shifts the image in 8 directions by a certain number of pixels, σ. Therefore creates $8n$ feature images."

As the background images have very different qualities, at least one classifier was created for each species to analyze all the images. The classifiers were firstly trained using between 7 to 14 images, by drawing at least one ROI of the background and of the classifier on each one of them (Figure 8).

A

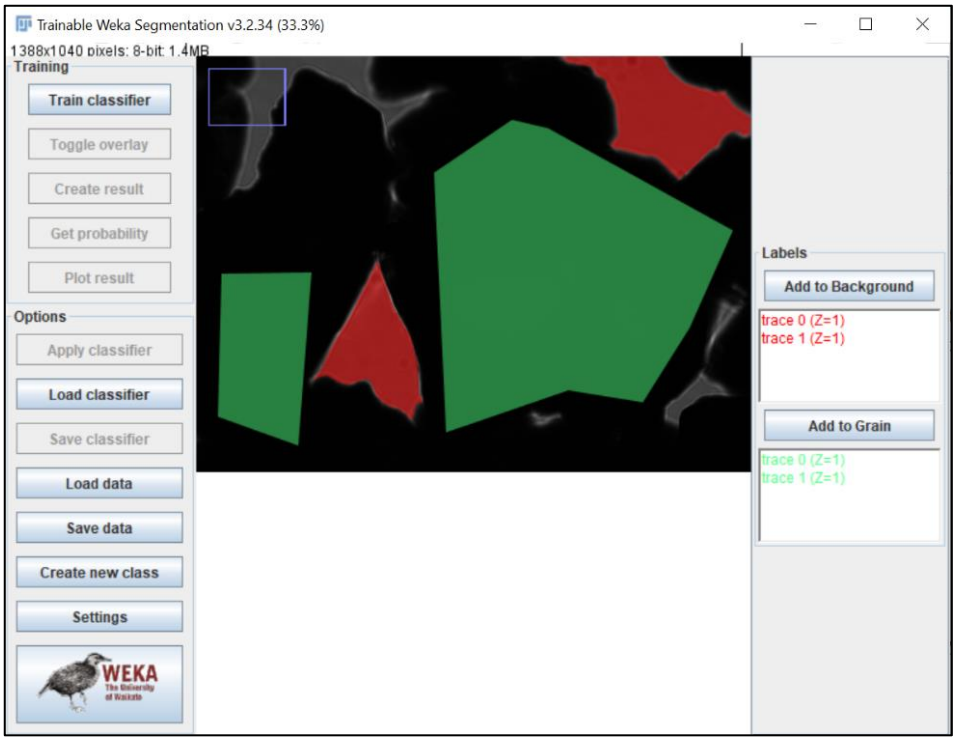

B

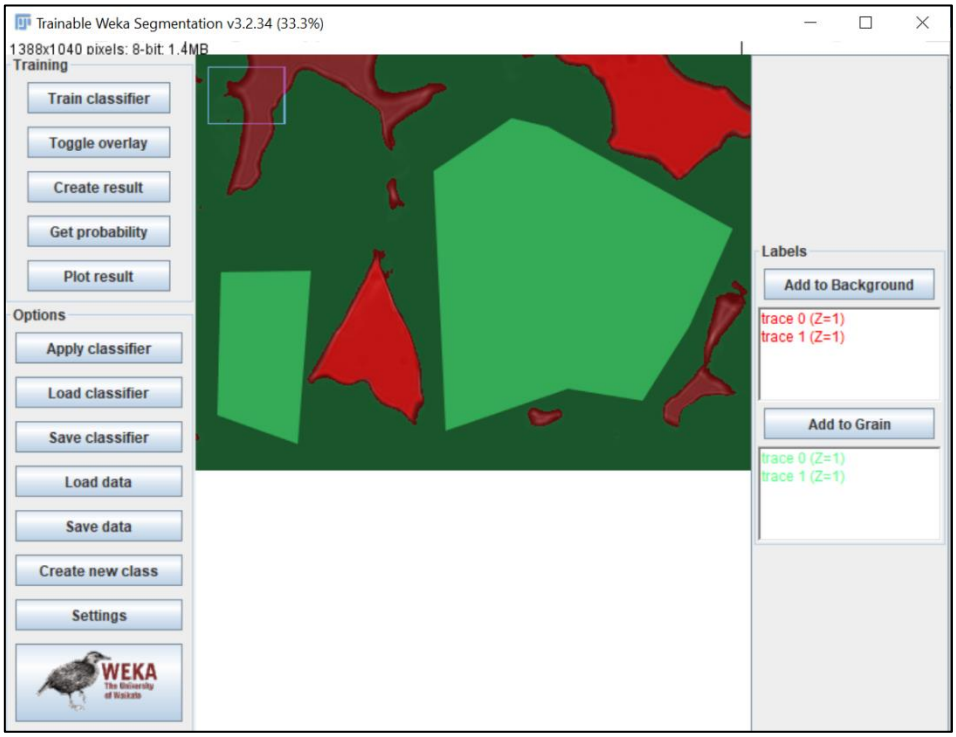

Figure 8: Training of the classifier. A) Classification of the region of interest B) Result of the training. In red : background area. In green : grain area.

Once the classifier reached a good accuracy, it was then tested on a set of 10 images to ensure their good functioning. Finally, the classifier was applied to the whole

set of images of the species through a batch process, using a Beanshell's script (Annex 2), a language similar to Java and to Fiji macro language. The open source script is available on the ImageJ website (*Scripting the Trainable Weka Segmentation*, 2020) and offers the possibility to analyze all the images present in a folder through a classifier, by choosing the input directory, the output directory, the classifier and the results (labels or probabilities). The results labels were chosen, to have a clear classification of the images

After the segmentation of the background images, the Otsu threshold method was applied, to finally calculate the size of the area through the "Analyze particle" plugin. The results were exported in a .csv file. This time, the size of the particles was set between 0 to infinity, to consider all area. The summary of the whole analysis of the background images is shown in Figure 9.

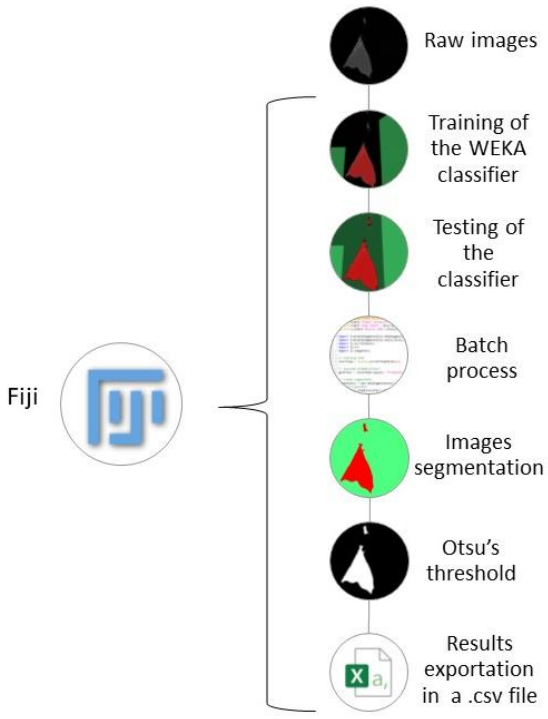

Figure 9: Summary of the methodology used for the analysis of the background images

4. Results and discussion

4.1. Colony counting

For a comprehensive analysis and quantification of biofilm formation by bioleaching bacteria, different methodology were implemented on the images. The first one is the application a primary treatment on the images, to improve their quality. As shown in Figure 10A, a high amount of noise was present on the photography, as quantity of images was probably more important than individual quality, when imaging was done. For this, the model DEFCoN, from the plugin DeepImageJ, was implemented to denoise the images and to highlight the fluorescent spots i.e., cells and colonies (Figure 10B).

The DEFCoN method does work well to treat the images containing only noise and which are not out of focus. It also allows to calculate the number of colonies more easily, as each cell spot is highlighted.

After the prior treatment of the images, the colonies were counting with Fiji and with a Python's script. With Fiji, the Otsu's method was used to have an automatic threshold. Due to the highlighting of the DEFCoN's model, the recognition of the colonies in the images is easily and well done. The threshold only amplifies the difference between the fluorescent spot underlined and the background, making the images to be countable through the plugin "Analyze particle". The results obtained after using this plugin are shown in the Figure 10C. For the Python's script, the thresholding and counting of the colonies is made simultaneously and the results are shown in the Figure 10D.

Both methods seem to give good results with small differences, but their processing is quite time consuming as it was necessary to primary treat the images

with DeepImageJ. Therefore, the images were analyzed as well through the Python's script without primary treatment. As the script uses the Laplacian of Gaussian with the blob_log algorithm, it does recognize fluorescent spots even if the image is noisy. An example of the image result is shown in Figure 10E.

To compare the different methods of counting, the results of colony counting for the four strains *A. ferridurans*^{T}, *L. ferrooxidans*^{T}, *A. ferriphilus*^{T} and *A. ferrooxidans*^{T} are plotted on graphs (Figure 11 and 12).

When the images were preliminary denoised, the counting between Fiji and the Python's script was similar for each of the four species (Figure 11). The difference in calculation is small and the behavior of the results was the same for the two methodologies. The major difference is that the number of colonies counted by Python seems to be higher than Fiji. Indeed, for *A. ferriphilus*^{T} (Figure 11A), the number of colonies calculated with the coded script is 12.5% higher than the one calculated through Fiji, for *A. ferridurans*^{T} it is 8.8% higher (Figure 11B), for *A. ferrooxidans*^{T} 7.4% higher (Figure 11C) and for *L. ferrooxidans*^{T} 7.9% higher (Figure 11D). These differences can be explained by the method used to count the colonies. Even if the colonies are priorly highlighted by the DEFCoN's model, their intensity can still vary. Therefore, the threshold of 0.1 used in the Laplacian of Gaussian detects probably more colonies than the automatic Otsu's method.

To compare colony counting with or without primary imaging denoising, the number of colonies identified were also plotted on graphs (Figure 12). For both methods, the counting was made through the Python's script. As for the comparison for the counting between Fiji and the script, the results are similar and the trends are the same. Indeed, the graphs show little differences between both methods. The

difference in percentage for the sum for each colony is about 1.9% for *A. ferriphilus*^{T} (Figure 12A), 15.9% for *A. ferridurans*^{T} (Figure 12B), 6.8% for *A. ferrooxidans*^{T} (Figure 12C) and 4.3% for *L. ferrooxidans*^{T} (Figure 12D). Clearly, the number of colonies counted by the script without denoising depends directly on the threshold implemented, therefore the difference of counting does not mean much, as it would vary depending on the threshold applied. However, it is important to highlight that the counting seems to work well even without having a denoising treatment of the images when the Python's script is used, making possible a straight analysis that can save time. Also, the two methods might calculate the same number of colonies, but it does not imply that the colonies counted are the same. Indeed, as the functions used to treat the images are different, fluorescent points that might not correspond to cell colonies can be considered as so. As stated before, the pyrite grains used here had a high amounts of quartz mineral and other impurities that are fluorescent under UV illumination and therefore can be counted as colonies.

An analysis of the X, Y positions of the colonies was conducted with the MATLAB's script to compare the location of the cells counted with and without previous denoising (Table 3).

Table 3 : Number and percentage of colocalized colonies counted by the script with and without prior denoising.

Species	*A. ferridurans*^{T}	*A. ferriphilus*^{T}	*A. ferrooxidans*^{T}	*L. ferrooxidans*^{T}
Number of colocalized colonies	513,493	373,667	832,699	713,729
Percentage of colocalized colonies	86.1%	82.3%	85.2%	87.0%

The percentage of colocalized colonies represent the ratio between the sum of colocalized colonies and the sum of colonies counted with the script for each species. For each strain, the ratio was between 82% and 87%. The variation of colonies counted

by both methodologies can be explained by the difference of thresholding and technique applied during the counting. For example, some of the grains of pyrite also contains pieces of quartz that are fluorescent on the images and that are accounted differently between both methodologies. On Figure 13A, it is possible to distinguish the quartz mineral on the upper right side of the raw image.

On the images containing quartz, the DEFCoN trained model does not recognize the entire impurity as a colony, as its size is too big, but the fluorescence of its borders is considered as so (Figure 13B).

The visual comparison of the Figure 13C and the Figure 13D show a different treatment of the quart's mineral between the analyses with or without denoising. When the image was directly analyzed with Python (Figure 13D), the center of the mineral is considered as colonies while mainly its borders are highlighted as so when the image was firstly denoised (Figure 13C). This highlighting of fluorescent spot can bias the results, by increasing the number of colonies counted. When the mineral is of a small size, the impact on the results might not be that important but could become relevant when the quartz covers a large area, overestimating the number of colonies counted on the grains. However, as the images of biofilms were done with the same pyrite batch, each set of images contained quartz and random impurities, this overestimation should be present in all datasets, and therefore should not have a strong impact when it comes to compare the results.

The percentage of colocalized colonies represent probably the real bacteria present on the grains and the rest of signals is probably due to quartz and other impurities. The percentage of colocalized colonies is close between each species,

meaning that the errors are probably the same for each culture and therefore should not have a significant impact in the results comparison.

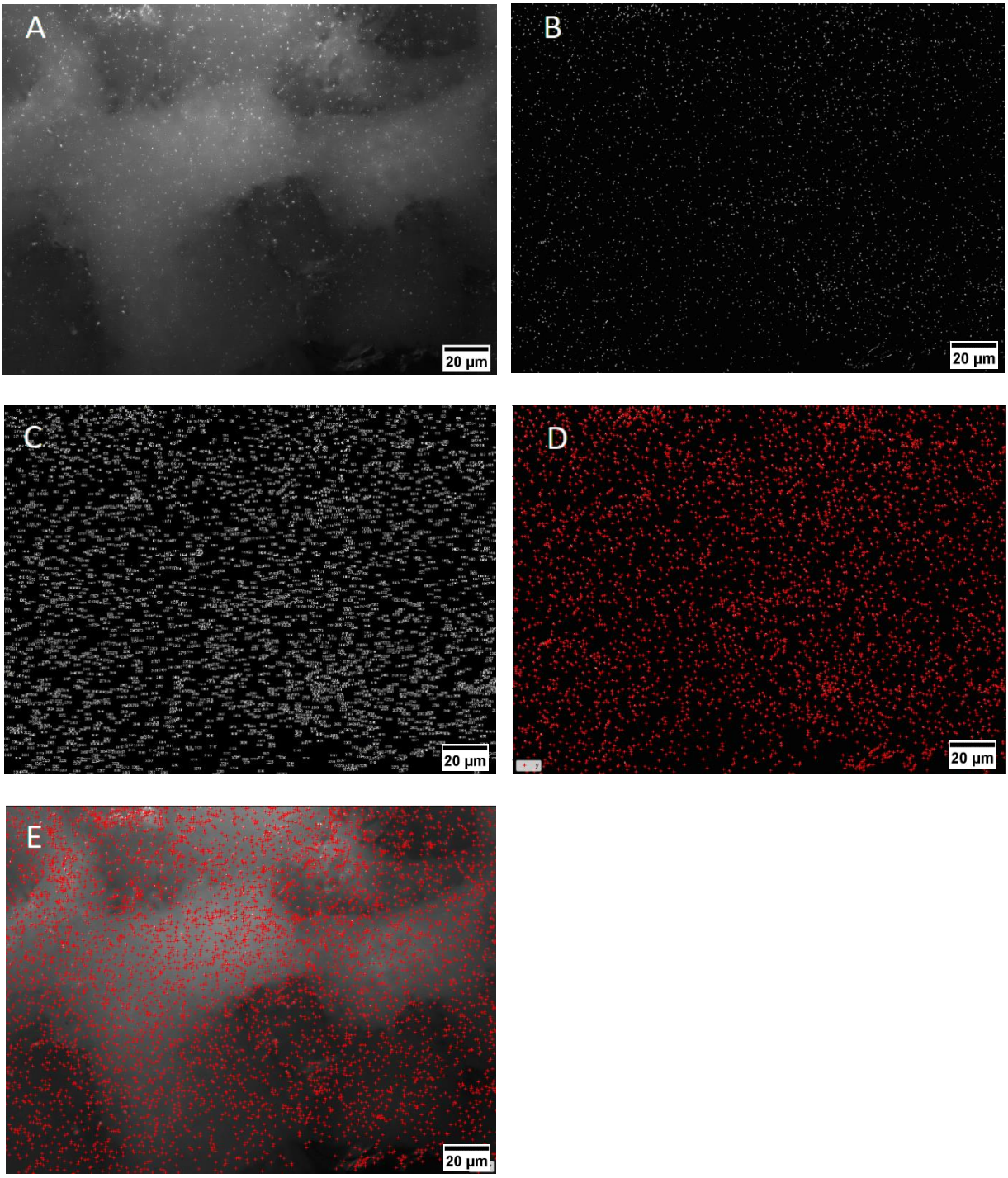

Figure 10: Fluorescent images of species *A. ferridurans*^{T} before and after denoising treatment. A) Raw image. B) Image after denoising through the DEFCoN model. C) Result of the colony counting through Fiji. D) Result of the colony counting through the Python's script with denoising. E) Result of the colony counting through the Python's script without denoising

.

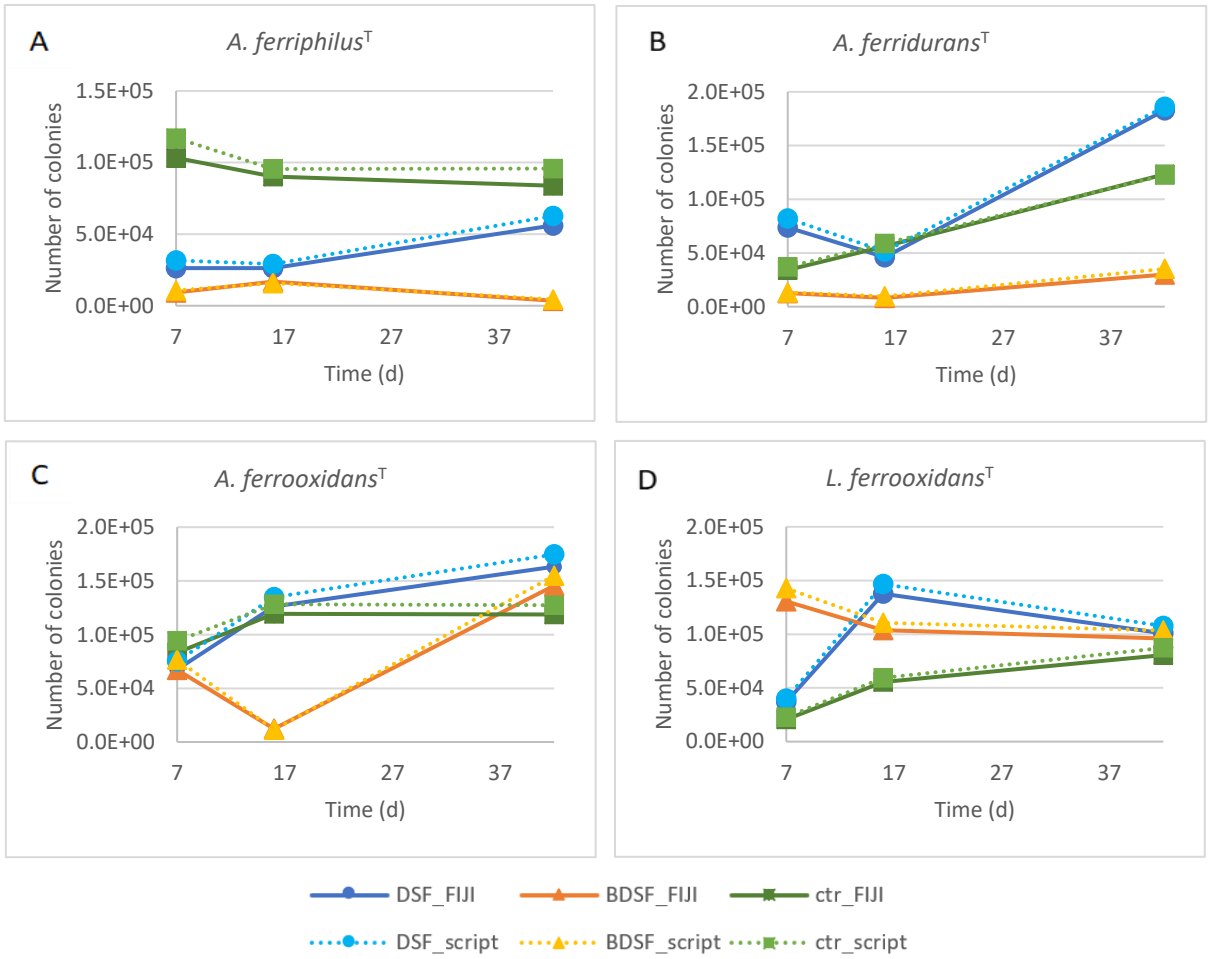

Figure 11 : Comparison of colony counting between the Python's script (teal, yellow and light green) and Fiji (blue, orange and dark green) for the control culture (square), culture with 5 µM DSF added at day 5 (circle) and culture with 5 µM BDSF added at day 5 (triangle). The cultures correspond of the strains A) *A. ferriphilus*^{T} ,B) *A. ferridurans*^{T}, C) *A. ferrooxidans*^{T} and D) *L. ferrooxidans*^{T}.

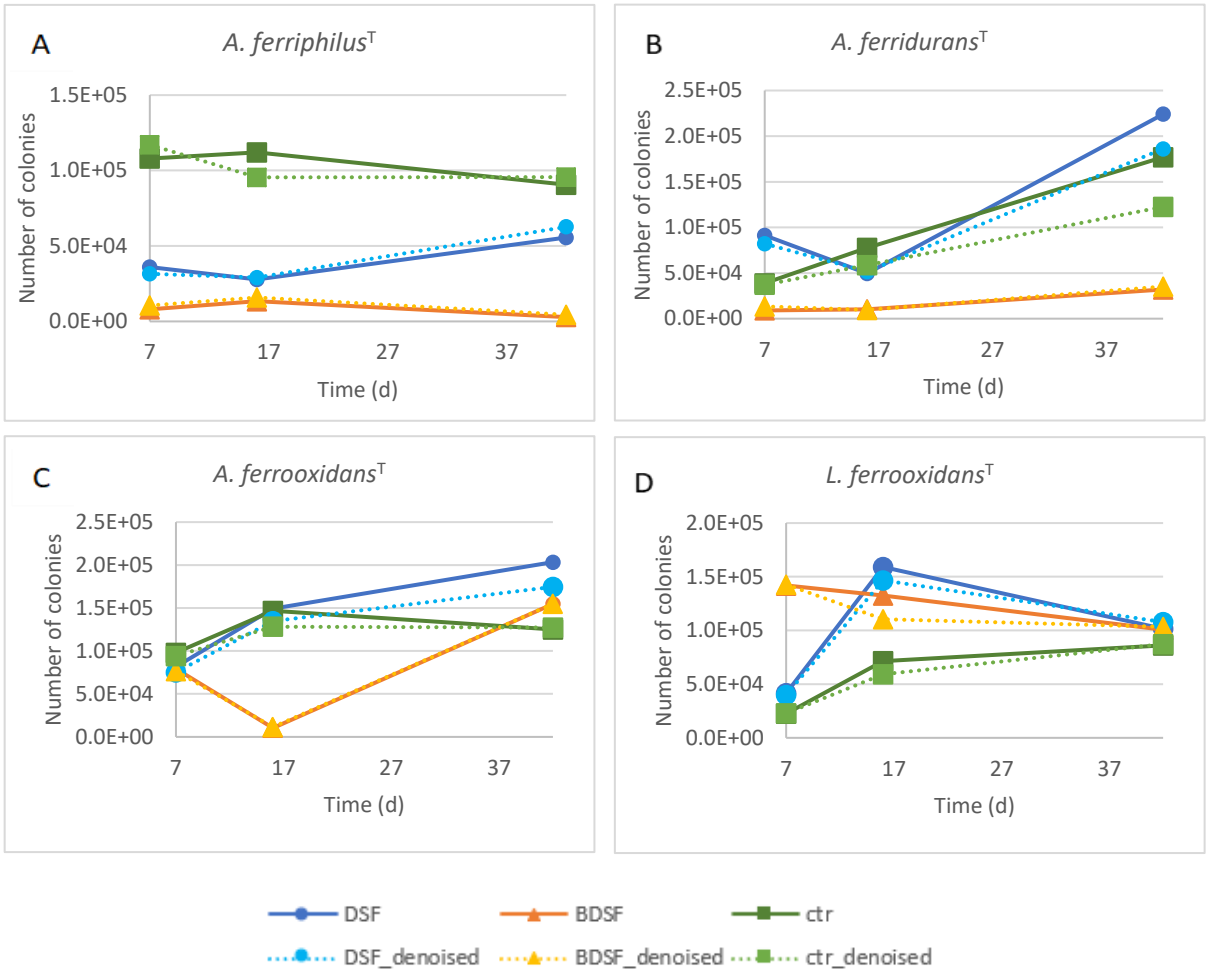

Figure 12: Comparison of colony counting with the Python's script with prior denoising of the images (teal, yellow and light green) and without prior treatment (blue, orange and dark green) for the strains A) *A. ferriphilus*^{T}, B) *A. ferridurans*^{T}, C) *A. ferrooxidans*^{T} and D) *L. ferrooxidans*^{T}, for the control culture (square), culture with 5µM DSF added at day 5 (circle) and culture with 5µM BDSF added at day 5 (triangle).

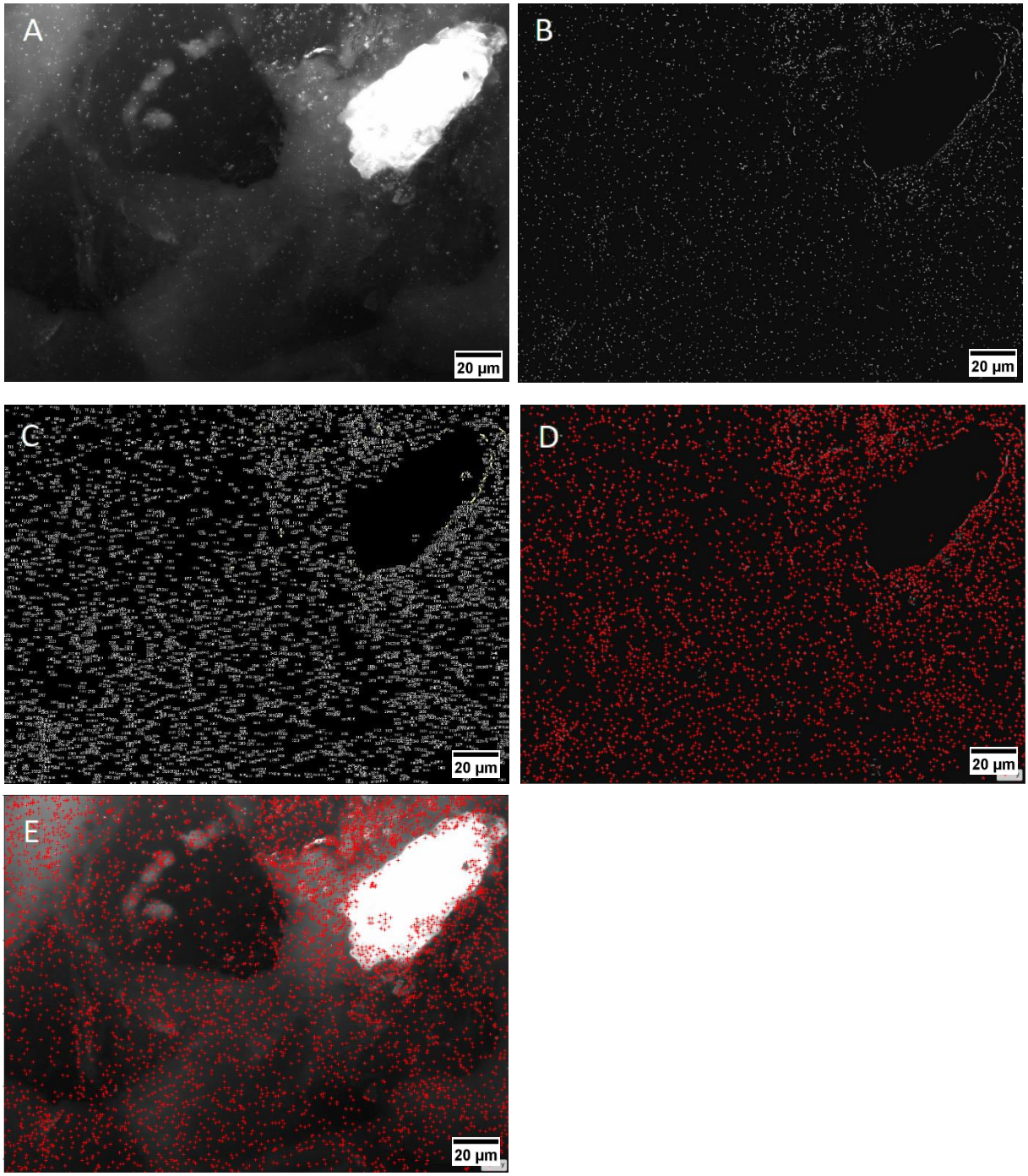

Figure 13 : Fluorescent images of *A. ferridurans*^{T} containing a piece of quartz, before and after denoising treatment. A) Raw image. B) Image after denoising through the DEFCoN model. C) Result of the colony counting through Fiji. D) Result of the colony counting through the Python's script with denoising. E) Result of the colony counting through the Python's script without denoising

4.2. Determination of grain area on images

The analysis of the grain area was conducted on the background images with the Trainable Weka Segmentation plugin of Fiji. The high-quality variation of the images does not allow a straight analysis with a simple threshold, as the results would be largely biased. Instead, the training of the segmentation plugin allowed to differentiate the background from the grain, a distinguishing that would be difficult to make without such software. Indeed, most of the background images show some noise or grain area with comparable pixel values than the background. Background images of different qualities are shown in Figure 14. Figure 14A shows a good differentiation between the background, in grey, and the grains, in black, with its corresponding Otsu's threshold (Figure 14B). On the other hand, the Figure 14C is an example where the difference between the grain and the background is not clear, with the corresponding Otsu's thresholding result (Figure 14D), showing the difficulty to apply a simple threshold to consider only the background. Segmentation was therefore needed, in order to have more accurate results (Figure 14E and 14F). But the high variation on the quality of images makes difficult to have a perfect segmentation on each image, even if classifiers were trained for each specie. Figure 15A shows an image with a high area of grains that can be considered as background with a simple thresholding method (Figure 15B), while the segmentation considers lower quantity of grain area as background, having less biased results (Figure 15C and 15D). The segmentation does therefore improve the analysis and ensure a better accuracy on calculation of grain areas. Furthermore, images of same qualities have already been evaluated in earlier studies (Bellenberg et al., 2018), and the background's images were treated only through a simple threshold. The segmentation implemented on this project will therefore present satisfying results.

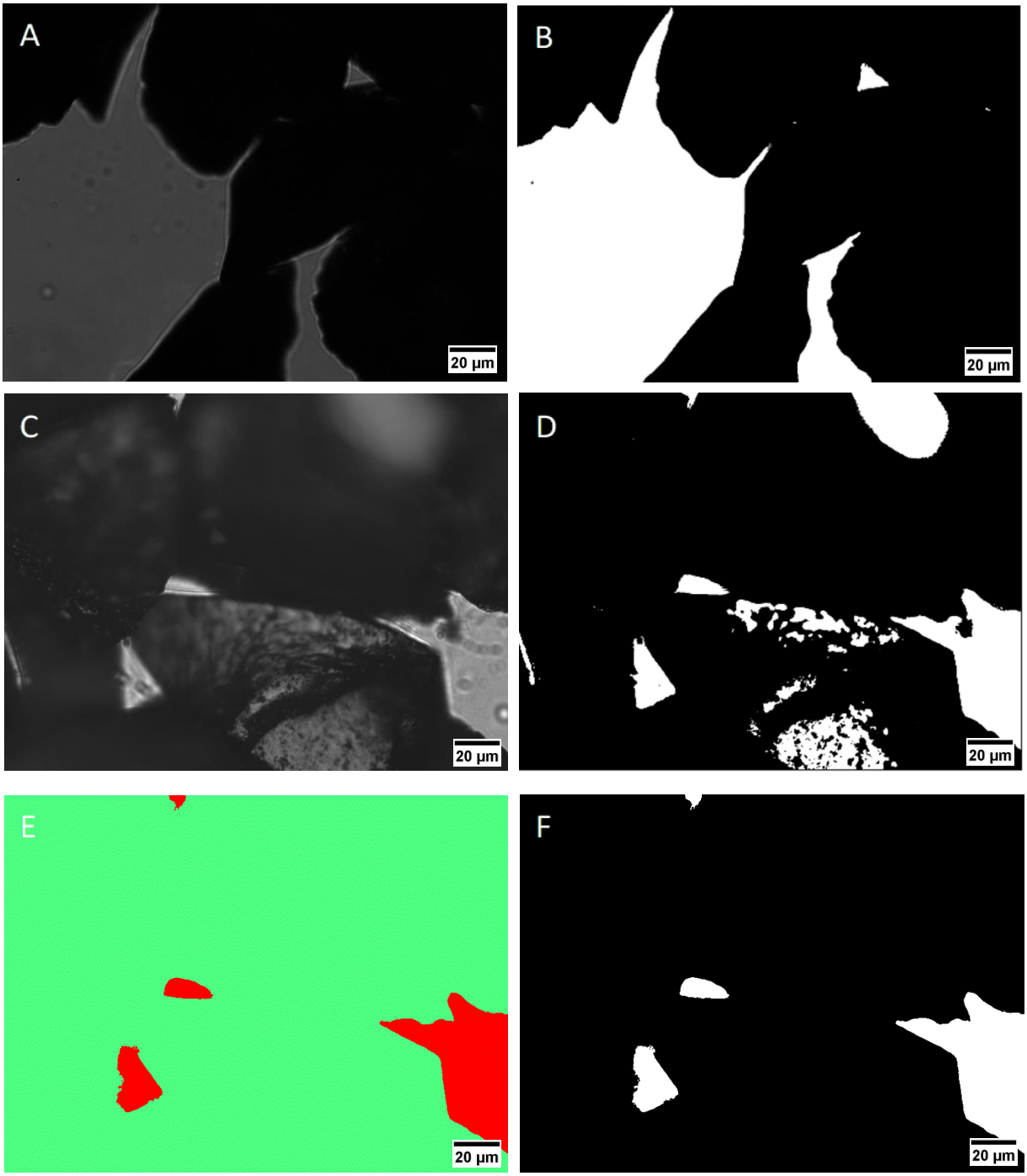

Figure 14: Example of background image with and without treatment. A) Raw image with a good differentiation between the background (grey) and the grain (black). B) Corresponding threshold of image A). C) Raw image with grain area. D) Corresponding threshold of image C). E) Image shown in C) after segmentation with the plugin Trainable Weka Segmentation. F) Threshold of image shown in E).

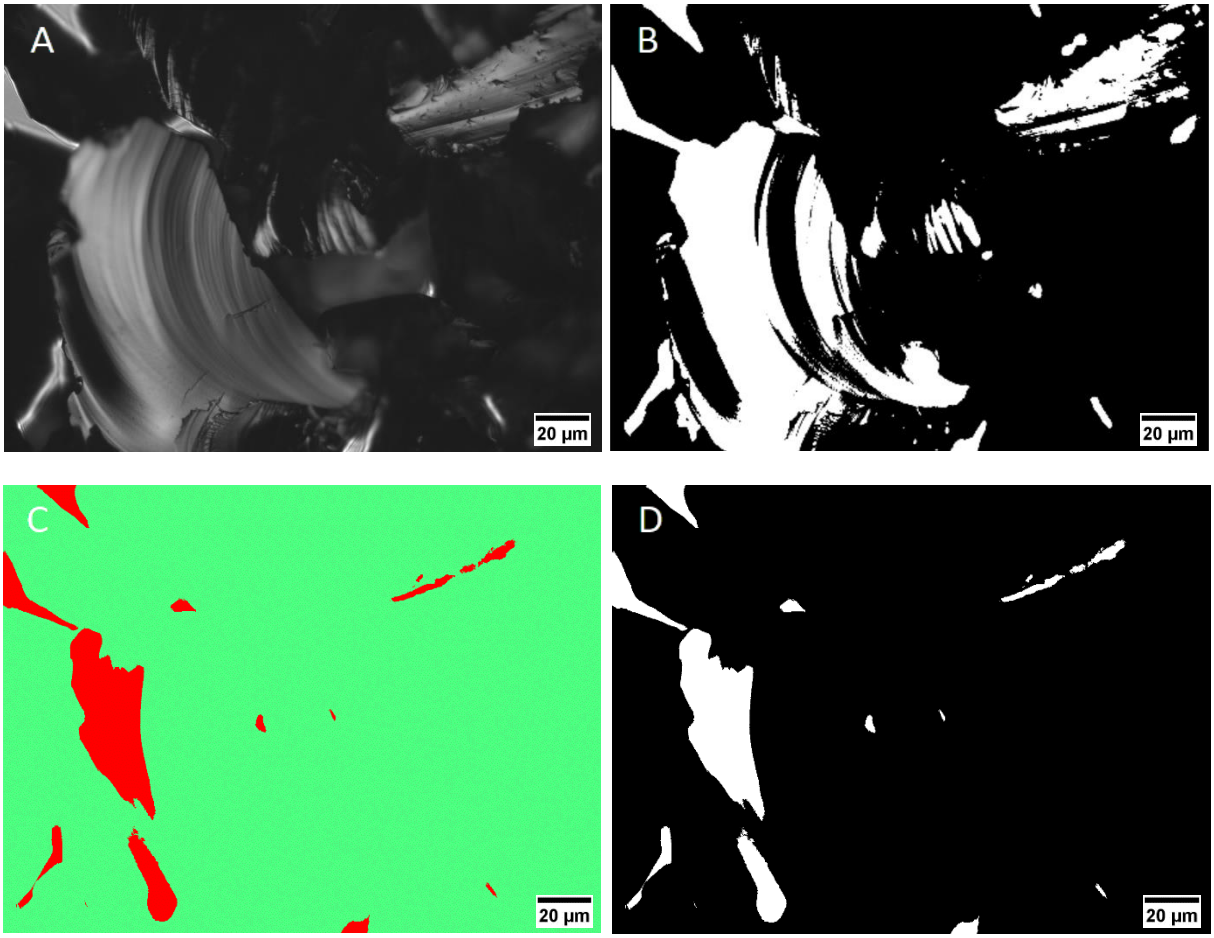

Figure 15 : Result of different thresholding for background determination of an image out of focus. A) Raw image. B) Corresponding thresholding of Image A). C) Image after segmentation with the plugin Trainable Weka Segmentation. D) Corresponding thresholding of Segmented image C)

4.3. Comparison of the images analysis techniques

With the analysis of the whole data set of images by Fiji and Python, it is possible to compare both techniques and to discuss their advantages and disadvantages for an automatic analysis of bioleaching biofilm images. The following table summarizes the important characteristics needed to treat the images.

Table 4: Comparison of automatic methodology using Fiji and Python to analyze biofilm images

	Fiji	Python
Colony counting	+	+
Analysis of background's images	+	+/-
Ease of use of the interface	+	+
Programing skills	+/-	-
Personalization of the analysis	+	+
Automatization	+	+
Time	+/-	+

Both methodologies can calculate the number of colonies, using different functions, even if the images present a high amount of noise or contains elements that decreases their quality. It is also possible to calculate the background area with both software when the images are of good quality and does not present noise, by using an automatic threshold. On the other hand, when the images are of poor quality and a trainable segmentation is needed, the Python's script shows its limit and cannot be easily used for such analysis, while Fiji and the different existing plugins can be more easily implemented. Indeed, the interface of Fiji is user-friendly and the different plugins available online permit to treat images in different ways. Python does also have an interface easy to use but it requires a lot of programing skills and knowledge to create a script. These skills are not needed to use Fiji, but they can provide a higher diversity of images analysis. Indeed, it allows to automatize the analysis of a whole dataset for

different plugins, as it has been done with the Beanshell's script to apply the Weka Segmentation to all the background's images. The personalization of the analysis is therefore feasible for both software, if the researcher has the programing skills. The most important characteristic of both software is that they can automatize the analysis, even though it can be time consuming for Fiji, as it is necessary to automatize plugin-by-plugin and it is complicated to embed them all in a script, as it can be done with Python.

The two methodologies employed are comparable in terms of functionality and they both work as expected to analyze a large set of images. However, the use of the Python's script is simpler and more efficient once it is written as only a few changes in the script are needed to run it for a whole set of data. Therefore, Python's script should rather be used when the images are of good quality as the analysis would be faster. In contrast, Fiji should be utilized when the images need a prior treatment before analysis.

4.4. Validation of the new quantification methodology

To corroborate the results obtained with the new methodology employed, another dataset from an experiment conducted on chalcopyrite was analyzed. This dataset was kindly provided by Dr. Bellenberg (Linnaeus University, Sweden). The objective of these experiments was to evaluate the impact of the addition of DSF_f on axenic and mixed cultures of the moderate leaching thermophiles, *A. caldus*^{T}, *L. ferriphilum*^{T} and *S. thermosulfidooxidans*^{T}. The quality of the images was the same than the one of pyrite analyzed previously, with a high amount of noise and fluorescent impurities.

The culture analyzed here are the axenic culture of *L. ferriphilum*^{T} (Figure 16 A and B) and the mixed culture of *L. ferriphilum*^{T} and *S. thermosulfidooxidans*^{T} (Figure 16 C and D). For the axenic culture, as shown in the published article, the methodology utilized in this project shows a drop of colonies right after the addition of DSF molecules, at day 5, and then an increase of population on days X, and Y. The behavior is therefore the same for both graphs, but our methodology shows a higher difference of growth between the cultures at day 12.

For the mixed culture of *L. ferriphilum*^{T} and *S. thermosulfidooxidans*^{T}, our methodology shows a drop of colonies at day 5 followed by an increase until day 12. Once again, the methodology used in this project shows a similar behavior than the article, with a lower difference between the two cultures at day 3 and a higher difference at day 12.

These differences are mainly due to the methodologies used in the counting of colonies as well as in the evaluation of grain area. Indeed, in Figure 17 is an illustration of the Python image analysis algorithm used in the article. The analysis of the

fluorescence images was made using a blob detection algorithm with Python in both researches, but different one; Bellenberg et al. (2018) used the Determinant of Hessian (blob_doh algorithm), while we used the Laplacian of Gaussian (blob_log algorithm) in this investigation. The Laplacian of Gaussian was preferred as it has a better accuracy for small blobs (< 3 pixels) than the Determinant of Hessian, leading to a more accurate analysis. For the analysis of the background images, the use of the Trainable Weka Segmentation plugin from Fiji allows to have a better appreciation of the grain area than the Otsu's threshold applied in the paper. These differences of methodologies used to analyze the images can lead to small differences within. Furthermore, after the analysis, Bellenberg et al. (2018) treated the data by removing the deciles of images with extremely low or high cell counts and by normalizing the images to 100% of mineral grain area.

The relative closeness of the results and of the conclusion that can be based on them shows that the methodology used in this thesis is working and proves to be reliable to quantify the development of biofilms over time.

L. ferriphilum^T

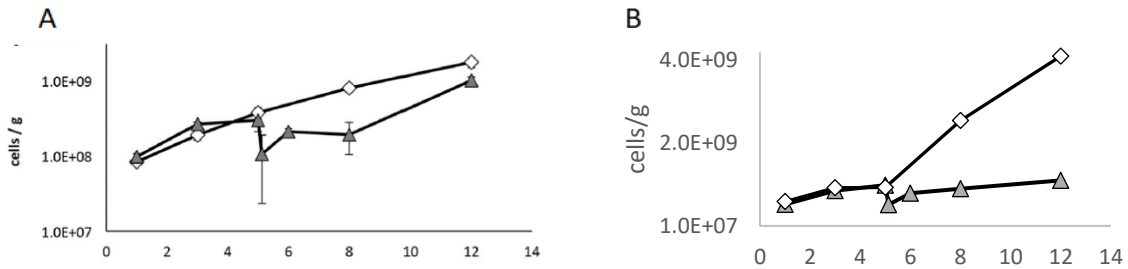

L. ferriphilum^T and *S. thermosulfidooxidans*^{T}

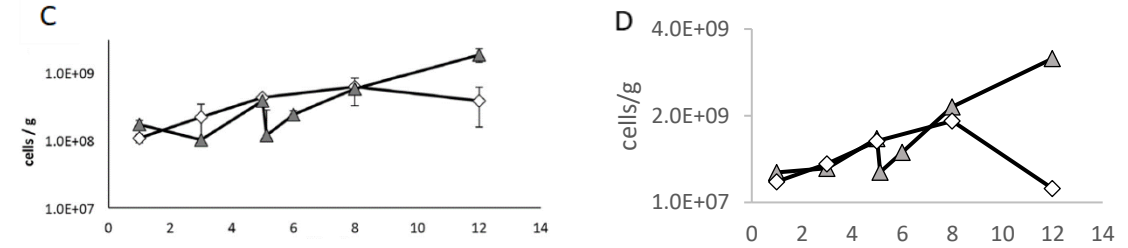

Figure 16 : Comparison of biofilm growth over time for the axenic culture of *L. ferriphilum*^{T} (A and B) and the mixed culture of *L. ferriphilum*^{T} and *S. thermosulfidooxidans*^{T} (C and D), between the results obtained in the paper of Bellenberg et al. (2018) (A and C) and the methodology used in this project (B and D). The grey triangles represent the culture where 5 µM DSF_f was added after day 5 and the white diamonds represent the control culture. Results are expressed in cells/g.

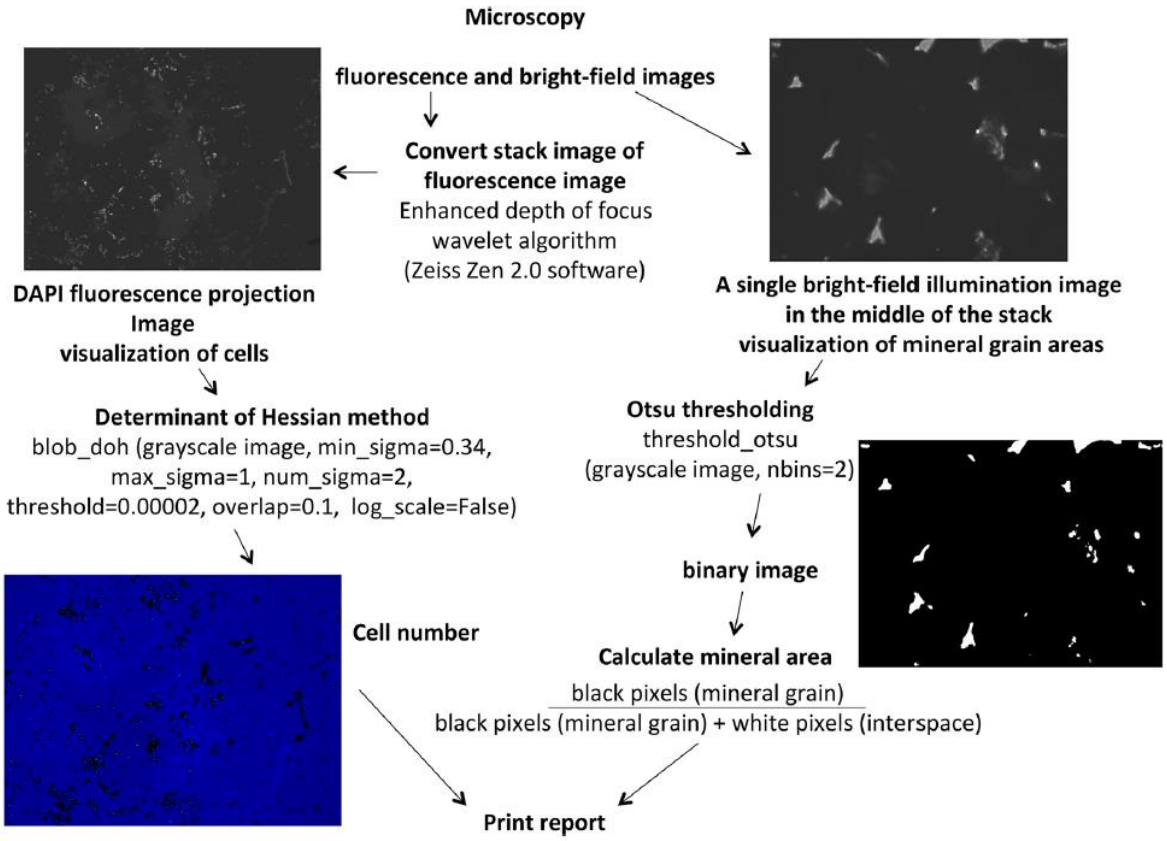

Figure 17 : Summary of the Python image analysis implemented in the paper of Bellenberg et al. (2018)

4.5. The effect of DSF and BDSF addition on *A. ferriphilus*^{T}, *A. ferridurans*^{T}, *A. ferridurans*^{T} and *L. ferrooxidans*^{T} cultures

To analyze the impact of the addition of DSF and BDSF on selected species of bioleaching bacteria, the number of colonies per grain area were quantified over time using the methodologies detailed in the previous sections. The colonies were analyzed through the Python's script without previous denoising of the images and the grain area was evaluated through the plugin Trainable Weka Segmentation in Fiji (Figure 18).

For *A. ferriphilus*^{T} (Figure 18A), the control culture has a quite steadily population from day 7 to day 42, with a significantly high population. Indeed, the number of colonies per area when 5 µM DSF and 5 µM BDSF are added at day 5 were lower than the one of the control culture during the whole experiment. These molecules seem to inhibit the growth of these species and even to decrease their population between day 7 and day 16 for cultures amended with DSF and between day 16 and 42 for cultures amended with BDSF. Bellenberg et al. (2018) have already emphasized that DSF molecules can slow the multiplication of axenic and mixed *L. ferriphilum*^{T} and *S. thermosulfidooxidans*^{T} and lead to the dispersion of the biofilm for some hours, but the bacteria did grow again after their dispersion and did not stagnate for days. It has also been shown that organic extracts of supernatants of *L. ferriphilum*^{T} biofilms, potentially containing DSF molecules, inhibit the oxidation of iron(II)-ions in several leaching microorganisms (Noël, 2013). Therefore *A. ferriphilus*^{T} could possibly have been affected by DSF and BDSF addition and have its capacity of iron(II)-ions oxidation inhibited.

For *A. ferridurans*^{T} (Figure 18B), when BDSF was added to the culture, the colonies did not grow as much as the other cultures. The number of colonies per area

increased from day 7 until day 42 but were all the time lower than in the control culture and the culture amended with DSF. The control culture grew steadily from day 7 until day 42, while the culture amended with DSF had a decrease of biofilm cell population from day 7 to day 16 and then an increase until day 42. The growth of *A. ferridurans*^{T} could be impacted by the BDSF molecules present in the culture as *A. ferriphilus*^{T} and probably was its ability to oxidize iron(II)-ions was inhibited at day 5. The DSF molecule does not seem to impact the biofilm growth of *A. ferridurans*^{T}.

In *A. ferrooxidans*^{T} (Figure 18C), the control culture increased its biofilm population from day 7 to day 16 and then cell counts decreased until day 42. The culture where DSF was added had the same rise of colonies from day 7 to day 16 and continues then until day 42. The addition of DSF seems not to impact the growth of *A. ferrooxidans*^{T} over time. In the culture where BDSF was added, the ratio colonies/area is the same as the other cultures at day 7 but dropped until day 16, before increasing until day 42. This drop could be due to the presence of BDSF inhibiting the growth of the bacteria and spreading the biofilm. Since no measurement was made before the addition of BDSF, it is not possible to ensure that the number of colonies was indeed higher at day 5 than at day 7 and decreased then until day 16 due to the presence of BDSF.

For *L. ferrooxidans*^{T} (Figure 18D), the control culture grew from day 7 until day 42. The culture amended with DSF at day 5 showed an increase of colonies from day 7 to day 16 and then a decrease from day 16 to day 42. The DSF could affect the bacteria and slow their biofilm growth before the day 7, spreading the biofilm. This spreading might lead to a better repartition of the bacteria over the grain and offering the cells new attachment sites and more space to grow. The population then decreased slowly until day 42. The colonies might have reached a density limit where colonies

start to die. The culture where BDSF was added after 5 days shows a high number of colonies per square micrometer at day 7. Probably this molecule seems not to affect biofilm growth of *L. ferrooxidans*^{T}. Then the population of colonies decreased until day 42.

It is also important to state that these experiments need to be repeated, as it is not possible to control the results due to the lack of technical replicas. Another important point is the lack of data before the addition of the DSF_f, making impossible to ensure that the three different cultures of each species had the same behavior before the day 5 ensuring a good development of the experiment.

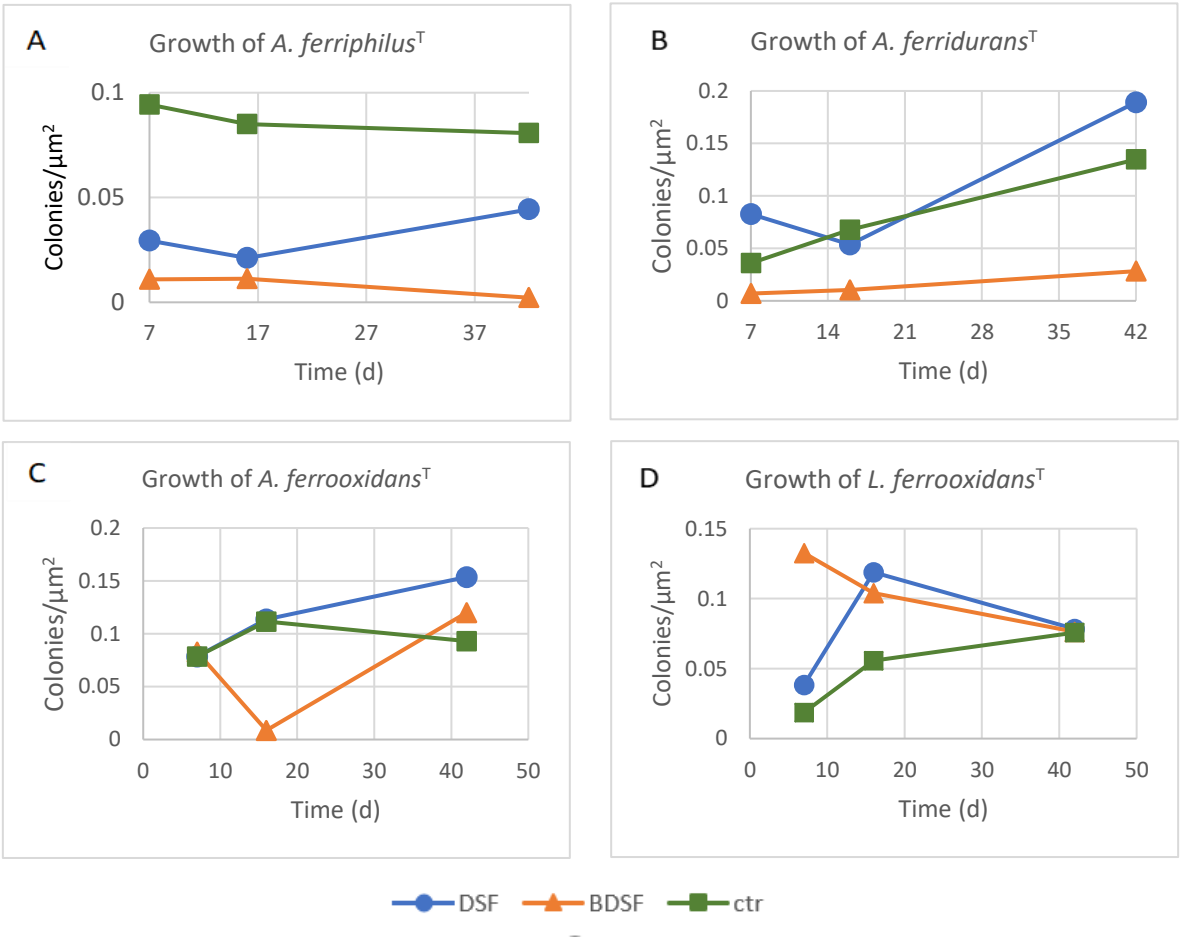

Figure 18 : Biofilm population dynamics of the species A) *A. ferriphilus*^{T}, B) *A. ferridurans*^{T}, C) *A. ferrooxidans*^{T} and D) *L. ferrooxidans*^{T} over time. Results are expressed in colonies/µm^2. Control cultures (green squares), cultures with addition of 5 µM DSF after 5 days (blue circles), cultures with addition of 5µM BDSF after 5 days (orange triangles).

5. Conclusions

The automatic images analysis methodology used in this project allows to have a trustful and open-source quantification of bioleaching bacterial biofilm for semi/quantitative analysis. Indeed, the methodology is validated by the dataset analyzed in the publication of Bellenberg et al. (2018), ensuring its good functioning and the results accuracy. High throughput automatic analysis imaging is essential to investigate bioleaching bacterial biofilm to have statistically robust results. This new quantification methodology can be freely use in future research on bioleaching bacterial biofilm and for the evaluation of microbial colonization on other minerals or solid particles. It can provide a basis for temporal analysis of axenic culture, but also of mixed cultures with different cell staining. The methodology can indeed be used to differentiate species depending on staining to analyze multispecies biofilm patterns, as it is possible nowadays to combine lipids, protein, DNA and/or lectins binding staining to differentiate species. This work can also help to improve machine learning analysis by feeding the deep neural network with verified data, leading to a deeper characterization of patterns and dynamisms of biofilms. Machine learning analysis would provide more robust statistical analysis by semi/quantitative analysis and help for the implementation of bioleaching in an industrial scale.

The analysis of bioleaching bacteria under the presence of DSF_f shows that some species are impacted by these molecules. Indeed, the colonization of metal sulfides by *A. ferriphilus*^{T} seems to be inhibited in presence of DSF and BDSF and the one of *A. ferridurans*^{T} seems also to be inhibited but only under the presence of BDSF. Due to the sanitary situation, the access to the laboratory was limited and it was not possible to validate these results with a new experiment. It would therefore be interesting to realize a similar experiment with the same species to corroborate the

results and to prove again that DSF_f can influence directly bioleaching, with images of good quality. Even if semi/quantitative analysis is important for a better understanding of bioleaching, imaging should not be underestimated as better analysis can be realized when the data are of good quality.

Bibliography

Aguilar, C., Carlier, A., Riedel, K., & Eberl, L. (2009). Cell–Cell Communication in Biofilms of Gram-Negative Bacteria. In R. Krämer & K. Jung (Eds.), *Bacterial Signaling* (1st ed., pp. 23–40). Wiley. https://doi.org/10.1002/9783527629237.ch2

Arganda-Carreras, I., Kaynig, V., Rueden, C., Eliceiri, K. W., Schindelin, J., Cardona, A., & Seung, H. S. (2017). Trainable Weka Segmentation: A machine learning tool for microscopy pixel classification. *Bioinformatics*, *33*(15), 2424–242. https://doi.org/10.1093/bioinformatics/btx18

Banerjee, G., & Ray, A. K. (2016). The talking language in some major Gram-negative bacteria. *Archives of Microbiology*, *198*(6), 489–499. https://doi.org/10.1007/s00203-016-1220-x

Bassler, B. L., & Losick, R. (2006). Bacterially Speaking. *Cell*, *125*(2), 237–246. https://doi.org/10.1016/j.cell.2006.04.001

Bellenberg, S., Buetti-Dinh, A., Galli, V., Ilie, O., Herold, M., Christel, S., Boretska, M., Pivkin, I. V., Wilmes, P., Sand, W., Vera, M., & Dopson, M. (2018). Automated Microscopic Analysis of Metal Sulfide Colonization by Acidophilic Microorganisms. *Applied and Environmental Microbiology*, *84*(20), e01835-18, /aem/84/20/e01835-18.atom. https://doi.org/10.1128/AEM.01835-18

Bellenberg, S., Díaz, M., Noël, N., Sand, W., Poetsch, A., Guiliani, N., & Vera, M. (2014). Biofilm formation, communication and interactions of leaching bacteria during colonization of pyrite and sulfur surfaces. *Research in Microbiology*, *165*(9), 773–781. https://doi.org/10.1016/j.resmic.2014.08.006

Bosecker, K. (1997). Bioleaching: Metal solubilization by microorganisms. *FEMS Microbiology Reviews*, *20*(3–4), 591–604. https://doi.org/10.1111/j.1574-6976.1997.tb00340.x

Brierley, C. L., & Brierley, J. A. (2013). Progress in bioleaching: Part B: applications of microbial processes by the minerals industries. *Applied Microbiology and Biotechnology*, *97*(17), 7543–7552. https://doi.org/10.1007/s00253-013-5095-3

Buades, A., Coll, B., & Morel, J.-M. (2011). Non-Local Means Denoising. *Image Processing On Line*, *1*. https://doi.org/10.5201/ipol.2011.bcm_nlm

Buetti-Dinh, A., Herold, M., Christel, S., El Hajjami, M., Bellenberg, S., Ilie, O., Wilmes, P., Poetsch, A., Sand, W., Vera, M., Pivkin, I. V., & Dopson, M. (2020). Systems biology of acidophile biofilms for efficient metal extraction. *Scientific Data*, *7*(1), 215. https://doi.org/10.1038/s41597-020-0519-2

Buetti-Dinh, A., Herold, M., Sand, W., Vera, M., Dopson, M., Pivkin, I. V., Wilmes, P., Boretska, M., Christel, S., Galli, V., Bellenberg, S., & Ilie, O. (2019). Deep neural networks outperform human expert's capacity in characterizing bioleaching bacterial biofilm composition. *Biotechnology Reports*, 5. https://doi.org/10.1016/j.btre.2019.e00321

Cheng, Z., He, Y.-W., Lim, S. C., Qamra, R., Walsh, M. A., Zhang, L.-H., & Song, H. (2010). Structural Basis of the Sensor-Synthase Interaction in Autoinduction of the Quorum Sensing Signal DSF Biosynthesis. *Structure*, *18*(9), 1199–1209. https://doi.org/10.1016/j.str.2010.06.011

Christel et al. - 2018—Multi-omics Reveals the Lifestyle of the Acidophil.pdf. (n.d.).

Comisión Chilena del cobre, E. (2020). *INDICADORES ECONÓMICOS DE LOS PRINCIPALES PAÍSES / BLOQUES CONSUMIDORES DE COBRE*. 4.

https://www.cochilco.cl/Mercado%20de%20Metales/MERC%202020%2011%2006.pdf

Darbon, J., Cunha, A., Chan, T. F., Osher, S., & Jensen, G. J. (2008). Fast nonlocal filtering applied to electron cryomicroscopy. *2008 5th IEEE International Symposium on Biomedical Imaging: From Nano to Macro*, 1331–1334. https://doi.org/10.1109/ISBI.2008.4541250

Della Sala, G., Teta, R., Esposito, G., & Costantino, V. (2019). The Chemical Language of Gram-Negative Bacteria. In *Quorum Sensing* (pp. 3–28). Elsevier. https://doi.org/10.1016/B978-0-12-814905-8.00001-0

Diao, M., Taran, E., Mahler, S., & Nguyen, A. V. (2014). A concise review of nanoscopic aspects of bioleaching bacteria–mineral interactions. *Advances in Colloid and Interface Science*, *212*, 45–63. https://doi.org/10.1016/j.cis.2014.08.005

Flemming, H.-C., Neu, T. R., & Wozniak, D. J. (2007). The EPS Matrix: The "House of Biofilm Cells." *Journal of Bacteriology*, *189*(22), 7945–7947. https://doi.org/10.1128/JB.00858-07

Flemming, H.-C., & Wingender, J. (2010). The biofilm matrix. *Nature Reviews Microbiology*, *8*(9), 623–633. https://doi.org/10.1038/nrmicro2415

Garnett, J. A., & Matthews, S. (2012). Interactions in Bacterial Biofilm Development: A Structural Perspective. *Current Protein and Peptide Science*, *13*(8), 739–755. https://doi.org/10.2174/138920312804871166

Gómez-de-Mariscal, E., García-López-de-Haro, C., Donati, L., Unser, M., Muñoz-Barrutia, A., & Sage, D. (2019). *DeepImageJ: A user-friendly plugin to run deep learning models in ImageJ* [Preprint]. Bioengineering. https://doi.org/10.1101/799270

González, A., Bellenberg, S., Mamani, S., Ruiz, L., Echeverría, A., Soulère, L., Doutheau, A., Demergasso, C., Sand, W., Queneau, Y., Vera, M., & Guiliani, N. (2013). AHL signaling molecules with a large acyl chain enhance biofilm formation on sulfur and metal sulfides by the bioleaching bacterium Acidithiobacillus ferrooxidans. *Applied Microbiology and Biotechnology*, *97*(8), 3729–3737. https://doi.org/10.1007/s00253-012-4229-3

Henderson, L. (2018). *Acid Mine Drainage: Chemistry, Effects and Treatment*. Nova Science Publishers, Incorporated. http://ebookcentral.proquest.com/lib/epflch/detail.action?docID=5497772

Kim, S.-R., & Yeon, K.-M. (2018). Quorum Sensing as Language of Chemical Signals. In *Comprehensive Analytical Chemistry* (Vol. 81, pp. 57–94). Elsevier. https://doi.org/10.1016/bs.coac.2018.03.010

Luisier, F., Vonesch, C., Blu, T., & Unser, M. (2010). Fast interscale wavelet denoising of Poisson-corrupted images. *Signal Processing*, *90*(2), 415–427. https://doi.org/10.1016/j.sigpro.2009.07.009

Martinez, P., Vera, M., & Bobadilla-Fazzini, R. A. (2015). Omics on bioleaching: Current and future impacts. *Applied Microbiology and Biotechnology*, *99*(20), 8337–8350. https://doi.org/10.1007/s00253-015-6903-8

Monnet, V., & Gardan, R. (2015). Quorum-sensing regulators in Gram-positive bacteria: ‘Cherchez le peptide ’: Quorum-sensing regulators in Gram-positive bacteria. *Molecular Microbiology*, *97*(2), 181–184. https://doi.org/10.1111/mmi.13060

Noël, N. (2013). *Attachment of acidophilic bacteria to solid substrata* (p. 116) [Dissertation]. Universität Duisburg-Essen. https://duepublico2.uni-

due.de/servlets/MCRFileNodeServlet/duepublico_derivate_00034699/Nanni_Noel_Dissertation.pdf

Obreque-Contreras, J., Pérez-Flores, D., & Gutiérrez, P. (2015). Acid Mine Drainage in Chile: An Opportunity to Apply Bioremediation Technology. *Journal of Waste Water Treatment & Analysis*, *06*(03). https://doi.org/10.4172/2157-7587.1000215

Rendueles, O., & Ghigo, J.-M. (2012). Multi-species biofilms: How to avoid unfriendly neighbors. *FEMS Microbiology Reviews*, *36*(5), 972–989. https://doi.org/10.1111/j.1574-6976.2012.00328.x

Rohwerder, T., Gehrke, T., Kinzler, K., & Sand, W. (2003). Bioleaching review part A: *Applied Microbiology and Biotechnology*, *63*(3), 239–248. https://doi.org/10.1007/s00253-003-1448-7

Ruiz, L. M., Valenzuela, S., Castro, M., Gonzalez, A., Frezza, M., Soulère, L., Rohwerder, T., Queneau, Y., Doutheau, A., Sand, W., Jerez, C. A., & Guiliani, N. (2008). AHL communication is a widespread phenomenon in biomining bacteria and seems to be involved in mineral-adhesion efficiency. *Hydrometallurgy*, *94*(1–4), 133–137. https://doi.org/10.1016/j.hydromet.2008.05.028

Sand, W., Gehrke, T., Jozsa, P.-G., & Schippers, A. (2001). *(Bio)chemistry of bacterial leaching-direct vs. Indirect bioleaching*. 17. https://doi.org/10.1016/S0304-386X(00)00180-8

Schindelin, J., Arganda-Carreras, I., Frise, E., Kaynig, V., Longair, M., Pietzsch, T., Preibisch, S., Rueden, C., Saalfeld, S., Schmid, B., Tinevez, J.-Y., White, D. J., Hartenstein, V., Eliceiri, K., Tomancak, P., & Cardona, A. (2012). Fiji: An open-

source platform for biological-image analysis. *Nature Methods*, *9*(7), 676–682. https://doi.org/10.1038/nmeth.2019

Schindelin, J., Rueden, C. T., Hiner, M. C., & Eliceiri, K. W. (2015). The ImageJ ecosystem: An open platform for biomedical image analysis: T HE I MAGEJ E COSYSTEM. *Molecular Reproduction and Development*, *82*(7–8), 518–529. https://doi.org/10.1002/mrd.22489

Schipper, B. W., Lin, H.-C., Meloni, M. A., Wansleeben, K., Heijungs, R., & van der Voet, E. (2018). Estimating global copper demand until 2100 with regression and stock dynamics. *Resources, Conservation and Recycling*, *132*, 28–36. https://doi.org/10.1016/j.resconrec.2018.01.004

Schippers, A. (2004). Biogeochemistry of metal sulfide oxidation in mining environments, sediments, and soils. *Special Paper of the Geological Society of America*, 15. https://doi.org/10.1130/0-8137-2379-5.49

Schippers, A., & Sand, W. (1999). Bacterial Leaching of Metal Sulfides Proceeds by Two Indirect Mechanisms via Thiosulfate or via Polysulfides and Sulfur. *Applied and Environmental Microbiology*, *65*(1), 319–321. https://doi.org/10.1128/AEM.65.1.319-321.1999

Schneider, C. A., Rasband, W. S., & Eliceiri, K. W. (2012). NIH Image to ImageJ: 25 years of image analysis. *Nature Methods*, *9*(7), 671–675. https://doi.org/10.1038/nmeth.2089

Scripting the Trainable Weka Segmentation. (2020). https://imagej.net/https://imagej.net/Scripting_the_Trainable_Segmentation

Vera, M., Schippers, A., & Sand, W. (2013). Progress in bioleaching: Fundamentals and mechanisms of bacterial metal sulfide oxidation—part A. *Applied*

Microbiology and Biotechnology, *97*(17), 7529–7541. https://doi.org/10.1007/s00253-013-4954-2

Zhang, R., Neu, T. R., Blanchard, V., Vera, M., & Sand, W. (2019). Biofilm dynamics and EPS production of a thermoacidophilic bioleaching archaeon. *New Biotechnology*, *51*, 21–30. https://doi.org/10.1016/j.nbt.2019.02.002

Zhou, J., & Cai, Z. (2018). Microbial Social Interactions in Biofilm. In Pallaval Veera Bramhachari (Ed.), *Implication of Quorum Sensing System in Biofilm Formation and Virulence* (pp. 29–46). Springer Singapore. https://doi.org/10.1007/978-981-13-2429-1_4

Zhou, L., Zhang, L.-H., Cámara, M., & He, Y.-W. (2017). The DSF Family of Quorum Sensing Signals: Diversity, Biosynthesis, and Turnover. *Trends in Microbiology*, *25*(4), 293–303. https://doi.org/10.1016/j.tim.2016.11.013

Annex

1. Python's script to analyze colony

This file extracts the data from an experiment folder and creates a file with the obtained information

```
%matplotlib inline
import matplotlib
import matplotlib.pyplot as plt
import numpy as np
import os.path
import glob
import pickle as pkl

#modify some matplotlib parameters to manage the images for illustrator
matplotlib.rcParams['pdf.fonttype'] = 42
matplotlib.rcParams['ps.fonttype'] = 42

from skimage.filters import gaussian
import skimage.feature as skfeat
from skimage.io import imread, imsave
from scipy import ndimage

import pandas as pd

Parameters to define
# Files to analyse
im_extension = 'jpg'
folder = '/Users/timrudge/Code/MarioVera/Denoised/'

# Parameters for analysis
smoothing_sigma = 0.5 # Radius of gaussian smoothing
min_colony_radius = 3 # Min radius of colony (pixels)
max_colony_radius = 20 # Max radius of colony (pixels)
threshold = 0.1 # Intensity threshold to detect colonies

Load Images
images = {}
```

```
files = os.listdir(folder)
images = {f: imread(os.path.join(folder, f)) for f in files}

Detect and record colony size and position
results = []
for file,im in images.items():
    sim = gaussian(im, smoothing_sigma)
    A = skfeat.blob_log(
        sim,
        min_sigma=min_colony_radius / np.sqrt(2),
        max_sigma=max_colony_radius / np.sqrt(2),
        num_sigma=10,
        threshold=threshold,
        overlap=0.2);
    y = A[:,0]
    x = A[:,1]
    r = A[:,2] * np.sqrt(2)
    result = pd.DataFrame()
    result['x'] = x
    result['y'] = y
    result['r'] = r
    result['file'] = file
    results.append(result)
results = pd.concat(results)

Check one of the files
file = 'A ferridur_33020_day42_BS-EF-Image Export-04_m01.jpg'
im = images[file]

# Show the image
fig,ax = plt.subplots(1, 1, figsize=(12,12))
ax.imshow(im)

# Plot the colony positions
results.plot(x='x', y='y', style='r+', ax=ax)
<matplotlib.axes._subplots.AxesSubplot at 0x7ff90fdc8fa0>
```

Count the colonies in each file and create csv file

results.groupby(‘file’)[‘x’].count()

results.to_csv(output_file_name)

2. Beanshell's script to implement the plugin Trainable Weka Segmentation to a whole dataset

```
#@ File(label="Input directory", description="Select the directory with input images", style="directory") inputDir
#@ File(label="Output directory", description="Select the output directory", style="directory") outputDir
#@ File(label="Weka model", description="Select the Weka model to apply") modelPath
#@ String(label="Result mode",choices={"Labels","Probabilities"}) resultMode

import trainableSegmentation.WekaSegmentation;
import trainableSegmentation.utils.Utils;
import ij.io.FileSaver;
import ij.IJ;
import ij.ImagePlus;

// starting time
startTime = System.currentTimeMillis();

// caculate probabilities?
getProbs = resultMode.equals( "Probabilities" );

// create segmentator
segmentator = new WekaSegmentation();
// load classifier
segmentator.loadClassifier( modelPath.getCanonicalPath() );

// get list of input images
listOfFiles = inputDir.listFiles();
for ( i = 0; i < listOfFiles.length; i++ )
{
   // process only files (do not go into sub-folders)
   if( listOfFiles[ i ].isFile() )
   {
      // try to read file as image
      image = IJ.openImage( listOfFiles[i].getCanonicalPath() );
      if( image != null )
      {
```

```
            // apply classifier and get results (0 indicates number of threads is auto-detected)
            result = segmentator.applyClassifier( image, 0, getProbs );

            if( !getProbs )
                // assign same LUT as in GUI
                result.setLut( Utils.getGoldenAngleLUT() );

            // save result as TIFF in output folder
            outputFileName = listOfFiles[ i ].getName().replaceFirst("[.][^.]+$", "") + ".tif";
            new FileSaver( result ).saveAsTiff( outputDir.getPath() + File.separator + outputFileName );

            // force garbage collection (important for large images)
            result = null;
            image = null;
            System.gc();
        }
    }
}
// print elapsed time
estimatedTime = System.currentTimeMillis() - startTime;
IJ.log( "** Finished processing folder in " + estimatedTime + " ms **" );
```

3. MATLAB's script to analyze the colocalized colonies

```
%%
clear
T_denoise = readtable('A.ferrooxidan detail.xlsx');
x1={};
y1={};
T_denoise_result=table();
for i=1:36
  name = {'A_ferroox 23270_day16_ctr-EF-Image Export-01_m01.jpg'
'A_ferroox 23270_day16_ctr-EF-Image Export-01_m02.jpg'
…
'A_ferroox 23270_day16_ctr-EF-Image Export-01_m36.jpg'
};
T_denoise_result=T_denoise(strcmp(T_denoise.file, name(i)), :);
x_1=(str2double(T_denoise_result.x));
y_1=(str2double(T_denoise_result.y));
x1(:,i)= {x_1};
y1(:,i)={y_1};
end
%%
T_raw = readtable('raw_A.ferrooxidans 23270_012.xlsx');
x2={};
y2={};
T_raw_result=table();
for i=1:36

T_raw_result=T_raw(strcmp(T_raw.file, name(i)), :);
x_2=(str2double(T_raw_result.x));
y_2=(str2double(T_raw_result.y));
x2(:,i)= {x_2};
y2(:,i)={y_2};
end
for j=1:36
n1(j)=numel(x1{1,j});
n2(j)=numel(x2{1,j});
end
```

```
% calculate all pairwise distances
%%
sum=0;
tic
for k=1:36
   changes = zeros(n1(k),n2(k));
for i = 1:n2(k)
    changes(:,i) = (x1{1,k}-x2{1,k}(i)).^2 + (y1{1,k}-y2{1,k}(i)).^2;
end
% find distances less than a given tolerance
tol = 9;
[j,o] = find(changes < tol);
l(k)=numel(j);
sum=sum+l(k);
end
toc
```